

The Ameliorative Potential of Alda-1 on Experimentally Induced Liver Fibrosis in Adult Male Mice. A Histological, Immunohistochemical and Biochemical Study

Amany A. Solaiman and Silvia Kamil Seddik Sawires

Department of Histology and Cell Biology, Faculty of Medicine, Alexandria University, Egypt

ABSTRACT

Introduction: Because of its complex pathogenesis, liver fibrosis remains one of the diseases with no standard treatment. Alda-1 is considered as a promising drug in ameliorating such fibrosis.

Aim of the Work: To evaluate the potential effect of Alda-1 after thioacetamide (TAA)-induced liver fibrosis in male mice.

Materials and Methods: Twenty-five adult male mice (25–27 gm aged 2-3 months) were allocated into five equal groups. Group I (control group), group II (Alda-1 group): each mouse was given Alda-1 [5 mg/kg, intraperitoneally (ip)] twice weekly for four weeks. Group III (TAA group): each animal received TAA (200 mg/kg, ip) twice weekly for seven weeks. Group IV (TAA +Alda-1 group): each mouse was given TAA as group III. After stoppage of TAA administration, Alda-1 was given at a dose as group II and continued for four weeks. Group V (recovery group) each animal received TAA treatment as group III and left without any treatment for an extra four weeks. The histological changes were identified by the light (H&E and Masson's trichrome stains) and electron microscopies, immunohistochemical and morphometric analysis. Blood samples were taken to evaluate the liver's function.

Results: TAA caused marked histological and biochemical attenuation of hepatocytes structure and function with significant increase in collagen deposition. In addition, TAA caused significant elevation of liver enzymes. In Alda-1 treated In Alda-1 treated group (IV), hepatocytes revealed nearly normal structure, significantly decreased the elevated liver enzymes and significant increase in reduced glutathione and decrease in malondialdehyde in liver homogenate. Alda-1 decreased the elevated transforming growth factor, collagen-1 gene expression and the area percentage of collagen. In addition, alpha smooth muscle actin was significantly reduced. The anti-inflammatory effects were also detected by the decrease in the interleukin-6 and tumor necrosis factor- α .

Conclusion: Alda-1 ameliorated TAA-induced liver fibrosis in mice. This might be due to its antioxidant, antifibrotic and anti-inflammatory effects.

Received: 19 April 2022, **Accepted:** 14 May 2022

Key Words: Alda-1, fibrosis, hepatocytes, histology, immunohistochemistry.

Corresponding Author: Amany A. Solaiman, MD, Department of Histology and Cell Biology, Faculty of Medicine, Alexandria University, Egypt, **Tel.:** +20 10 9636 6227, **E-mail:** amansolaiman@gmail.com

ISSN: 1110-0559, Vol. 45, No. 3

INTRODUCTION

Liver fibrosis is the most important health problem nowadays. It affects more than 100 million individuals all over the world with an alarming prevalence of mortality^[1]. Liver fibrosis is the common reaction to a diversity of insults. This includes hepatitis B and C virus infection, as well as long-term exposure to toxins, chemicals or even drugs. In addition, chronic cholestatic diseases, metabolic diseases, and autoimmune diseases all might contribute to the production of liver fibrosis^[2].

Liver fibrosis if neglected might progress to hepatic cirrhosis, hepatocellular carcinoma, and eventually liver failure^[3]. Hepatic stellate cell (HSCs) activation is crucial for the progression of liver fibrosis^[4]. Activated HSCs directs the excessive deposition of certain proteins that would be accumulated within the extracellular matrix (ECM). One of the most important of these proteins is collagen type 1, as well as a variety of pro-inflammatory cytokines^[5]. Additionally, the disruption in the activity of

transforming growth factor- β 1 (TGF- β 1) is incredibly a robust effector in liver fibrosis^[6].

Thioacetamide (TAA) is a hepatotoxic agent utilized to cause a consistent, dose- and time- related liver fibrosis in experimental animals, resembling that realized in human^[7,8]. Its biotransformation to thioacetamide sulfoxide, which is metabolized and converted to thioacetamide disulfoxide, a highly toxic compound and efficient in modifying the cellular macromolecules. Oxidative stress, the buildup of reactive oxygen species (ROS), and cytotoxicity are the results of such modification. The mitochondria are well known to be affected. As such, excessive ROS may lead to buildup of reactive aldehydes which can precisely damage cellular protein leading to liver fibrosis^[9,10]. Aldehydes are detoxified by the aldehyde dehydrogenase family. Recently, a well characterized aldehyde dehydrogenase-2 (ALDH-2) activator, Alda-1 [N-(1,3-benzodioxol-5-ylmethyl)-2,6-dichlorobenzamide], works to stimulate ALDH2 catalytic property by altering ALDH2's kinetic characteristics and enhancing the substrate-enzyme interaction^[11,12]. It has

a valuable role in defending against certain diseases, as ischemic heart disease, stroke and alcoholic liver disease which might be facilitated through regulating oxidation stress and ROS production. Nevertheless, it might have a key role in preventing apoptosis and autophagy^[13,14].

Hence, the present study was established to determine the possible involvement of Alda-1 in attenuating thioacetamide – induced liver fibrosis in mice.

MATERIALS AND METHODS

Experimental animals

The animal house, Faculty of Medicine, Alexandria University, provided a total of twenty-five adult male mice (25–27 grammes) aged 2-3 months. Mice were given seven days to acclimate to the laboratory environment before starting the experiment. The animals were maintained in a temperature-controlled environment (25 °C) with light/dark cycles and free access to basic laboratory food and water. The experiment was carried out pursuant to a protocol that has been approved by the Committee of Animal Care's ethics committee. The Alexandria University Faculty of Medicine's Local Ethics Committee approved all the methods used. IRB number 00012098.

Chemicals

Thioacetamide (TAA) and Alda-1 were bought from Sigma-Aldrich (Sigma–Aldrich, USA)

Experimental design

Five groups of five mice in each were allocated at random:

1. Group I (control group): each animal was given a saline solution intraperitoneally (ip) twice weekly at a dose of 0.01 mg/kg body weight for seven weeks^[15].
2. Group II (Alda-1 group): each mouse was given Alda-1 ip twice weekly for four weeks at a dose of 5 mg/kg body weight^[16].
3. Group III (TAA group): 200 mg/kg body weight was given ip twice weekly for seven weeks to each animal of this group^[15].
4. Group IV (TAA + Alda-1 group): As in group III, each animal received TAA twice weekly for seven weeks. Following the cessation of TAA treatment, the animals were given Alda-1 (5 mg/kg body weight, ip) twice weekly for four weeks.
5. Group V (recovery group): each mouse was given TAA treatment as group III and left without any treatment for an extra four weeks.

Assessment of liver functions

Blood samples were taken to evaluate the liver's function. The retro-orbital plexus was used to collect the samples at the end of each group's allotted study period. After allowing the blood to coagulate, it was centrifuged

for 15 minutes at 3000 rpm. The aspartate transaminase (AST) and alanine transaminase (ALT) levels in the serum were measured using the Biodiagnostic kit from Cairo, Egypt.

Liver homogenate^[17]

Pieces of hepatic tissue were bathed in ice-cold phosphate buffered saline (PBS, pH=7.4). Tissue pieces were weighed before being homogenized [tissue weight (g): PBS (mL) volume=1:9]. To obtain the supernatant, the suspension was sonicated and centrifuged for 5 minutes at 5000 g. The samples were then kept at -80°C for biochemical assessment. A portion of the homogenate was promptly frozen in liquid nitrogen and maintained at a temperature of -80 °C for gene expression analysis.

Biochemical analysis

All biochemical tests were conducted at the Biochemistry department, Faculty of Science, Borg El-Arab, Alexandria University.

Malondialdehyde (MDA)^[18]

The reaction of MDA with thiobarbituric acid (TBA) was performed using a Bio diagnostics kit from Cairo, Egypt. The red pink colour of the resulting thiobarbituric acid reactive compounds (TBARS) was detected at 532 nm.

Reduced glutathione (GSH)^[19]

Using a BIOXYTECH kit, the quantities of GSH in liver homogenates were measured colorimetrically (Sigma, USA). At 412 nm, the resulting yellow colour was measured.

Tumor Necrosis Factor-alpha (TNF- α)^[20]

TNF- α was measured in the liver homogenate using the sandwich enzyme-linked immunosorbent assay (ELISA) technology (MyBioSource, San Diego, UK). In brief, biotinylated anti-rat TNF- antibody was added and incubated for one hour at 37 °C. The avidin-biotin combination was added, then incubated for half an hour at 37 °C. The 3,3',5,5'-Tetramethylbenzidine (TMB) colour development agent was then applied, and the absorbance was measured at 450 nm after a half-hour incubation at 37 °C in the dark.

Interleukin- 6 (IL-6)^[21]

ELISA kits were used to determine the levels of the inflammatory cytokine IL-6 in all animals in accordance with the manufacturer's procedure (Biosciences, San Diego, USA). As detection antibodies, anti-IL-6 polyclonal antibody was used, and biotin conjugated anti-IL-6 polyclonal antibody was used. TMB substrate was added after the avidin-biotin-peroxidase complex was introduced. At 450nm, the absorbance was measured.

Transforming Growth Factor- beta 1 (TGF- β 1)^[22]

TGF- β 1 levels were measured using an ELISA kit on hepatic tissue homogenate (MyBioSource, San Diego,

USA). The biotinylated anti-rat was added and incubated for one hour at 37 ° C. After that, the TMB colour development agent was applied and rinsed. For half an hour, the samples were incubated at 37 °C in the dark. At 450nm, the absorbance was read.

RNA extraction, cDNA synthesis and Real-Time Polymerase Chain Reaction (PCR)^[23]

The total RNA was isolated from the liver tissue homogenate using the TRIsure™ Lysis Reagent corresponding to the manufacturer's guidelines. The commercial first strand cDNA synthesis kit was used to make cDNA from 1 g of total RNA (SensiFAST cDNA Synthesis kit). The relative gene expression of collagen type I in comparison to the internal control gene, β -actin, was determined using the SensiFAST SYBR No-Rox kit for real-time PCR analysis. The thermal cycling protocol was as follows: denaturation (95 °C for two minutes), amplification (forty cycles, five seconds at 95 °C), annealing (ten seconds at 60 °C), and extension (twenty seconds at 72 °C). The threshold cycle (Ct) data were used to calculate the RNA concentration. The levels of mRNA expression were estimated in relation to the mRNA levels of the β -actin gene. Primer sequence (Sigma Aldrich): Collagen type I, F- 5'-TTCCTGCCTCAGCCACCTCA-3', R-5'- GAACCTTCGCTTCCATACTCG-3'; β -actin, sense: 5'-TGAGAGGGAAATCGTGCGT-3', anti-sense 5'-TCATGGATGCCACA GGATTCC-3'.

Histological examination

There were no deaths among the experimental animals. Specimens from the liver of each animal were carefully collected from each animal at the end of the experiment and divided into two portions. One was immersed in a 10% formal saline solution and processed to obtain paraffin sections of 4-5 μ m thickness^[24]. The sections were stained with hematoxylin and eosin (H&E) in addition to the Masson's trichrome stain and viewed by the light microscope (Olympus, Japan) supplied with a digital camera (Olympus, Japan).

The other part was immediately cut into small pieces (~1x1 mm³) and fixed in 3% phosphate-buffered glutaraldehyde before being processed for transmission electron microscopic examination^[25] using Joel 1400 plus electron microscope (Tokyo, Japan) at Faculty of Science, Alexandria University.

Immunohistochemical assessment^[26]

Alpha-smooth muscle actin (α -SMA) antibody was achieved (Biotecnologies, California, USA), with antigen retrieval (EDTA solution) addition. After that, 0.3 % hydrogen peroxide and protein block were added, and the mixture was incubated with rat anti α -SMA antibody (1: 200). After incubation with anti-rat IgG secondary antibodies (1:500), diaminobenzidine (DAB) chromogen was used to visualize the results. As a counterstain, hematoxylin was utilized. Leiomyoma was employed as a positive control.

Quantitative morphometric analysis

Using the NIH Fiji programme (NIH, Bethesda, USA), the following parameters were evaluated: Images acquired from Masson's trichrome stained slides at x100 were used to calculate the area % of collagen. Images recorded at x100 were used to calculate the area % of α -SMA. Measurements were obtained at random from five different fields from each mouse for each of these two parameters. The acquired information was given in the form of a mean and standard deviation (SD).

Statistical analysis^[27]

The data was entered into the computer and examined with version 20.0. SPSS is a software suite from IBM (Armonk, NY: IBM Corp). The mean, SD, and median were used to represent the quantitative data. The significance of the acquired results was assessed at a 5% level of significance. For regularly distributed quantitative data, the ANOVA test was employed to compare more than two groups. For pairwise comparisons, the Post Hoc test (Tukey) was utilized.

RESULTS

Liver enzymes (AST, ALT)

After seven weeks of TAA treatment (group III), AST and ALT liver enzymes were significantly elevated compared to group I and group II (control group and Alda-1 group). After Alda-1 treatment in group IV (TAA+ Alda-1 group), the AST and ALT levels depicted a significant reduction. Regarding group V (recovery group), the significant increase in AST and ALT levels were persisted in comparison to the control and Alda-1 groups (Figures 1 A,B respectively).

Biochemical results

Malondialdehyde (MDA)

MDA levels in tissue homogenate were found to be significantly higher in group III (TAA group) as compared to groups I and II (control and Alda-1 groups respectively) which showed no statistical difference among them. Meanwhile, Alda-1 treatment in group IV revealed a significant reduction in MDA levels compared to group III. The levels of MDA showed significantly higher levels in groups V (recovery group) compared to group I and group II as shown in (Figure 2A).

Reduced glutathione (GSH)

The mean amounts of GSH in the homogenate were significantly lower in group III (TAA group) compared to groups I and II (control and Alda-1 groups respectively). The levels in group IV (TAA+Alda-1 group) were significantly increased compared to group III. Furthermore, the levels in group V (recovery group) were significantly lower than those in groups I and II, but significantly higher than those in group III (Figure 2B).

Tumor Necrosis Factor -alpha (TNF- α)

When compared to the control and Alda-1 groups (groups I and II respectively), TNF- α levels in group III (TAA group) were considerably higher. Treatment with Alda-1 in group IV (TAA+Alda-1 group), there was a significant decrease in TNF- α levels in comparison to group III. The levels in group V (recovery group) were significantly increased compared to group I and group II (Figure 2C).

Interleukin 6 (IL 6)

Group III (TAA group) revealed significantly upregulated levels of IL-6 compared to the control group (group I) and Alda-1 (group II). Moreover, ameliorative effects after administration of Alda-1 in group IV (TAA+Alda-1 group) caused a significantly decreased IL-6 levels. In group V (recovery group) the levels of IL-6 were still significantly elevated compared to group I and group IV (Figure 2D).

Transforming Growth Factor -beta 1 (TGF- β 1)

When compared to the control and Alda-1 groups, TGF- β 1 levels were increased significantly in group III. In comparison to group III, group IV (TAA+Alda-1 group) had much significantly lower levels. TGF- β 1 levels were also significantly higher in group V (recovery group) compared to groups I and IV (Figure 2E).

Real-Time Polymerase Chain Reaction (PCR)

Expression of collagen type I gene was significantly increased in TAA-treated group (group III) compared to group I (control group) and group II (Alda-1 group) which showed no statistical difference among them. Providentially, following TAA treatment, Alda-1 resulted in a considerable decrease in collagen type I expression in group IV. In group V (recovery group) the collagen gene expression level was significantly increased compared to groups I and II (Figure 2F).

Histological results

Hematoxylin and eosin stain (H&E)

Group I (Control group): Examination of group I (control group) revealed normal liver structure. The hepatocytes were established in cords radiating from the central veins. Portal tracts were frequently seen. (Figures 3A,B). The hepatocytes showed eosinophilic cytoplasm and vesicular, centrally positioned nuclei (Figures 3B,C). Sometimes, binucleate hepatocytes were observed (Figure 3C). The cords of hepatocytes were interspaced with the hepatic sinusoids. The sinusoids exhibited narrow elongated slit like spaces with few bulging Kupffer cells (Figure 3C).

Group II (Alda-1 group): Microscopic examination revealed normal hepatic architecture with hepatocytes extending from the central veins (Figure 4A). The hepatocytes showed eosinophilic cytoplasm and central nuclei with prominent nucleoli (Figures 4 B,C). Many

hepatocytes were binucleated. Kupffer cells were also depicted bulging in the narrow sinusoids (Figure 4C).

Group III (TAA group): Following TAA treatment, light microscopic examination showed marked disruption of the normal hepatic architecture. Hepatic stroma demonstrated noticeable fibrous tissue septa. Many septa were seen arising from most of the portal areas and even some bridging from portal area to the neighboring portal area (Figure 5A). Moreover, mononuclear cellular infiltration was depicted (Figures 5A,B). Hepatocytes exhibited immense degenerative changes. Some hepatocytes showed hypereosinophilic cytoplasm and deeply stained nuclei (Figure 5B). Many hepatocytes were markedly swollen and ballooned with vacuolated cytoplasm (Figures 5 C,D). Nuclear changes were noticed, many hepatocytes showed deeply stained nuclei (Figures 5 B,C,D). Other showed complete or partial loss of nuclear chromatin (karyolysis) (Figures 5 C,D). The portal area revealed apparent proliferation of the bile ducts (Figure 5C).

Group IV (TAA+ Alda-1group): Interestingly, pronounced improvement was demonstrated in this group. The hepatic parenchyma in most examined sections revealed apparently normal hepatic architecture. The hepatocytes exhibited evident improvement. Hepatocytes were one or two cell thick cords radiating from the central veins and separated by hepatic sinusoids (Figures 6 A-D). Most hepatocytes appeared having eosinophilic cytoplasm and vesicular nuclei with prominent nucleoli (Figures 6 B-D). Moreover, many hepatocytes were binucleated (Figures 6 C,D). Whereas few appeared having small deeply stained nuclei and slightly vacuolated cytoplasm (Figures 6 B,D). Even though there was marked decrease in the inflammatory cellular infiltration, still some areas revealed mild cellular infiltration (Figures 6 A,C,D).

Group V (Recovery group): Connective tissue septa with evident lobulation (Figure 7 A) accompanied with cellular infiltration were observed (Figures 7 A-C). Meanwhile, the hepatocytes were still noticeably affected. Many hepatocytes appeared swollen with markedly vacuolated cytoplasm (Figures 7 B,C). In addition, some nuclei were small deeply stained (Figures 7 B,C) and others were karyolytic (Figure 7B).

Masson's trichrome stain

The stained stroma was prominent only around the vessels in the portal tracts and around the central veins in the control group (group I) and in group II (Alda-1 group) (Figures 8 A,B respectively). Group III (TAA group) showed that collagen was aggressively deposited around the portal tracts. Clearly some areas depicted septa extending from one portal tract to the adjacent one. In addition, the liver sections detected collagen deposition in between the hepatocytes (Figure 8C). The collagen deposition was markedly reduced after administration of Alda-1 in group IV (Figure 8D). Group V (recovery group) revealed persistent collagen deposition bridging from one portal tract to the other (Figure 8E).

Quantitative morphometric analysis of the area percentage (%) of collagen deposition

Values obtained from morphometric analysis of the area % of collagen deposition statistically corroborated the findings. When compared to the control and Alda-

1 groups (groups I and II respectively), mice in group III (TAA) showed a significant increase in area % of collagen deposition. In comparison to group III, group IV (TAA+Alda-1 group) showed a significant reduction in the area % of collagen deposition. In comparison to group III, the area % of collagen deposition was much higher in the recovery group (Figure 8F).

Immunohistochemical results of α -smooth muscle actin (α -SMA)

By immunohistochemistry, α -SMA positive reaction was weakly detected group I (control group). At higher magnification the brown positive reaction was exclusively expressed at the portal tracts and around the central veins. The reaction was nearly negative in between the hepatocytes (Figures 9 A-C). Similarly, α -SMA brown positive reaction was weakly detected in group II (Alda-1 group) to be only around the central veins and the portal tracts (Figures 9 D-F). In group III (TAA group) the reaction was clearly and strongly expressed in the connective tissue septa connecting some adjacent portal tracts (Figure 9G). The α -SMA positive reaction was evidently strong in the perisinusoidal area between the hepatocytes (Figures 9 H,I). Group IV (TAA+Alda-1 group) revealed marked reduction of the positive brown reaction which was restricted to the central veins and portal tracts (Figure 9K). Nevertheless, sporadic areas of positive reaction in the perisinusoidal spaces in between the hepatocytes were seen (Figures 9 L,M). In group V (recovery group), the positive reaction was strongly expressed in the connective tissue septa connecting many portal tracts with lobulation (Figure 9N). In addition, the perisinusoidal spaces expressed intense positive reaction (Figures 9 Q,R).

Quantitative morphometric analysis of the area % of α -SMA

The area % of α -SMA expression significantly increased in group III (TAA group) compared to group I and II (control and Alda-1 groups) which showed no statistical difference among them. Furthermore, the area % of positive immunostaining of α -SMA in group IV was dramatically reduced compared to group III. A significant increase was noted in group V (recovery group) as compared to the control and Alda-1 groups. (Figure 9T).

Electron microscopic results

Group I (Control group): More detailed exploration of hepatic structural organization was provided by the electron microscopic examination. Group I (control group) revealed hepatocytes presented with rounded large central nuclei, dispersed chromatin, and prominent nucleoli (Figure 10A). Numerous mitochondria scattered

in the cytoplasm (Figures 10 A-D), few profiles of rough endoplasmic reticulum flattened cisternae (Figure B) and smooth endoplasmic reticulum were seen as well (Figure 10C). Furthermore, stored glycogen appeared as aggregated electron dense granules in the cytoplasm (Figure 10D). Hepatocytes with projecting microvilli in the Disse space, as well as Kupffer cells in the hepatic sinusoids, were also seen (Figure 10E).

Group II (Alda-1 group): Electron microscopic examination revealed hepatocytes with rounded central nuclei and prominent multiple nucleoli. Few cytoplasmic vacuolations were seen (Figure 11A). The cytoplasm showed profiles of the rough endoplasmic reticulum (Figure 11B). Numerous mitochondria with prominent cristae were seen scattered in the cytoplasm (Figures 11B,C).

Group III (TAA group): Fine structure of the liver of TAA treated group exhibited histological alterations and degenerated hepatocytes that were referred to nearly all the cytoplasmic organelles and cytoplasmic rarefaction was also evident (Figures 12 A-D). Some hepatocytes showed disrupted cell membrane (Figures 12 C,D). Mitochondria were polymorphic with ill-defined outer membrane, and the organelles were clumped together (Figures 12 A,B) and some mitochondria appeared bizarre shaped (Figure 13A). Some mitochondria appeared with loss of their cristae and disrupted membrane (Figure 13B). Collagen fibrils were also seen (Figures 12D, 13C).

Group IV (TAA +Alda-1 group): Furthermore, electron microscopic findings of liver treated with TAA and Alda-1 demonstrated hepatocytes with nearly normal microscopic appearance as their cytoplasm contained euchromatic nuclei and prominent nucleoli and slightly irregular nuclear envelope (Figures 14 A,B). The cytoplasm of the hepatocytes revealed some vacuoles (Figures 14 A,B), numerous profiles of the rough endoplasmic reticulum (Figure 14C) and lysosomes (Figure 14B). The mitochondria were numerous with prominent cristae (Figures 14 B,C,D). In addition, bile canaliculi were seen as well (Figure 14B). Few collagen fibrils were seldomly seen adjacent to an elongated cell suggestive of a fibroblast (Figure 14E).

Group V (Recovery group): Ultrastructure examination was performed to assess the hepatic fibrosis and the spontaneous recovery from the induced histological changes after one month from stopping TAA administration. Notably, the histological changes and collagen deposition were still observed, indicating that the TAA-induced microscopic alterations persisted even after discontinuation of TAA treatment. The hepatocytes showed irregular nuclei (Figures 15 A-C) and cytoplasmic rarefaction (Figures 15 A-D) and lysosomes as well (Figure 15D). The mitochondria were dramatically affected where in some cells the mitochondria appeared with ill-defined out line and amalgamated together

(Figures 15 A,B). Some mitochondria showed loss of cristae (Figure 15E). Collagen deposition extracellularly

also persisted and even some areas intermingled with elastin deposition. (Figures 15A,F).

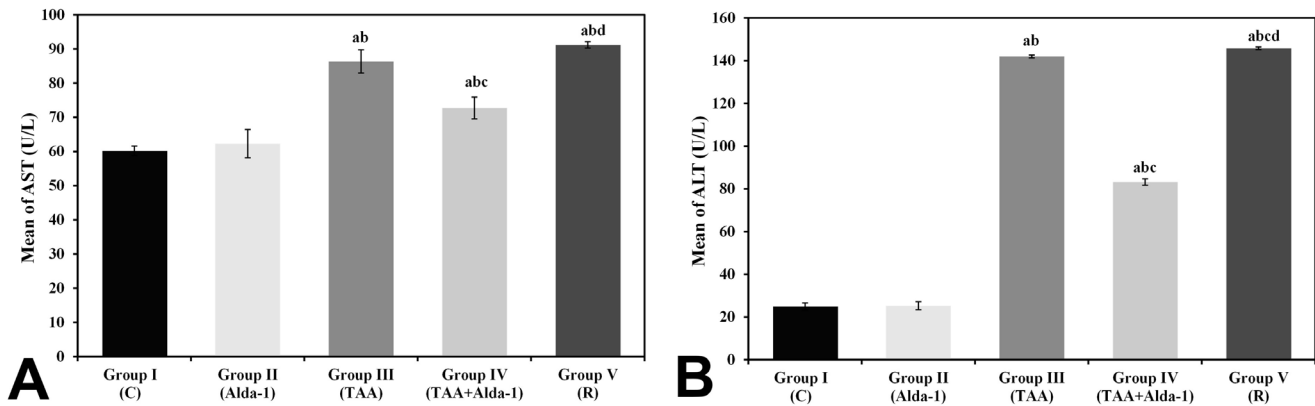


Fig. 1: (A, B): Bar charts representing comparative statistical analysis of the levels of AST and ALT liver enzymes.

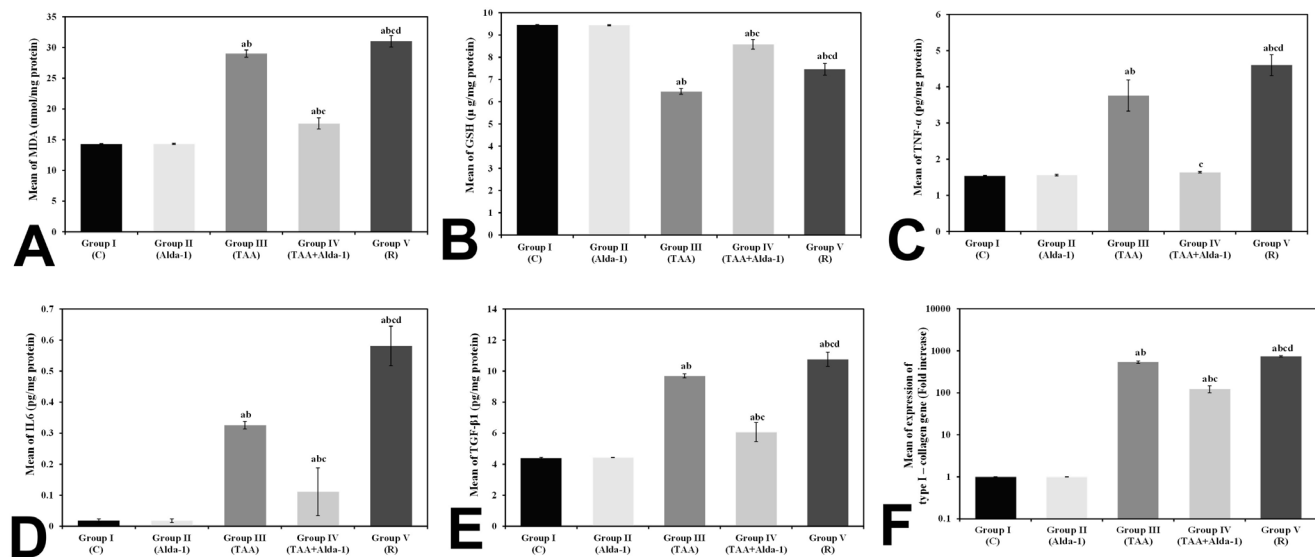


Fig. 2: (A-F): Bar charts representing comparative statistical analysis of liver homogenate of the following: A; Malondialdehyde (MDA), B; Reduced glutathione (GSH), C; Tumor Necrosis Factor-alpha (TNF-α), D; Interleukin 6 (IL-6), E; Transforming Growth Factor-beta 1 (TGF-β1) and F; Bar chart representing statistical analysis of gene expression of collagen type I.

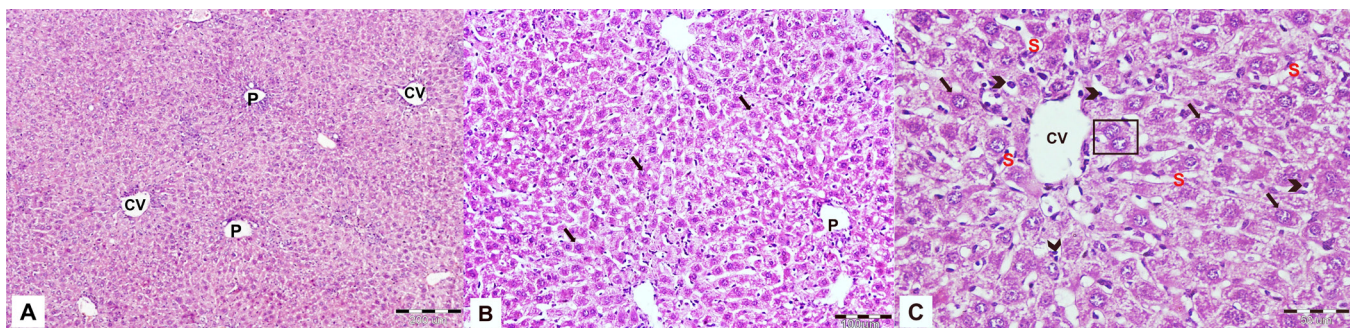


Fig. 3 (A-C):H&E-stained sections of the control group showing: A: Hepatocytes are regularly arranged around the central vein (CV). P; portal tract. B: The hepatocytes reveal eosinophilic cytoplasm with central nuclei (black arrow). P; portal tract. C: The cords of cells radiating from the central vein (CV). The hepatocytes are separated with elongated sinusoids (S). Few hepatocytes appear binucleated (square). Black arrow; vesicular nucleus, black chevron arrow; Kupffer cells. A x100, B x 200, C x 400.

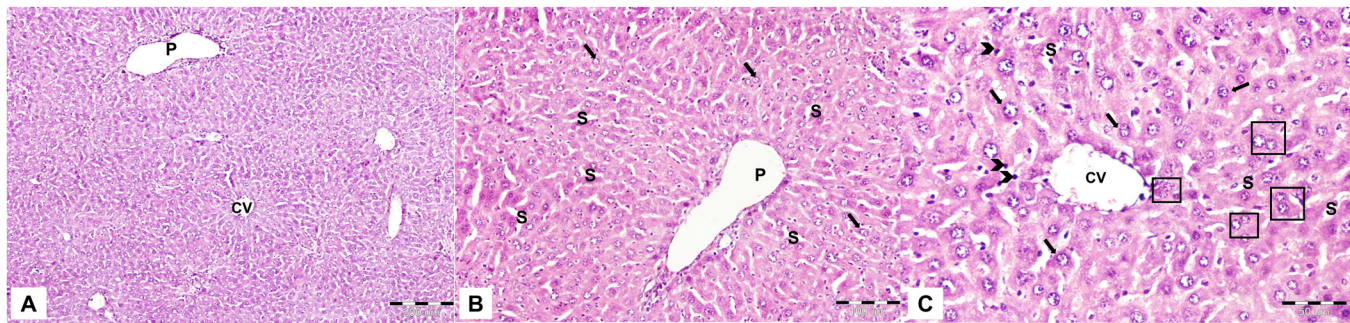


Fig. 4 (A-C): H&E-stained sections of group II (Alda-1 group) showing **A:** From the central vein, hepatocyte cords radiate (CV). P; portal tract. **B:** The hepatocytes reveal eosinophilic cytoplasm and central vesicular nuclei with prominent nucleoli (black arrow). P; portal tract, S; hepatic sinusoids. **C:** The hepatic sinusoids (S) are narrow and Kupffer cells are seen (black chevron arrows). Many hepatocytes are binucleated (square). The hepatocytes show eosinophilic cytoplasm and central vesicular nuclei with prominent nucleoli (black arrow). CV; central vein. A x100, Bx 200, Cx 400.

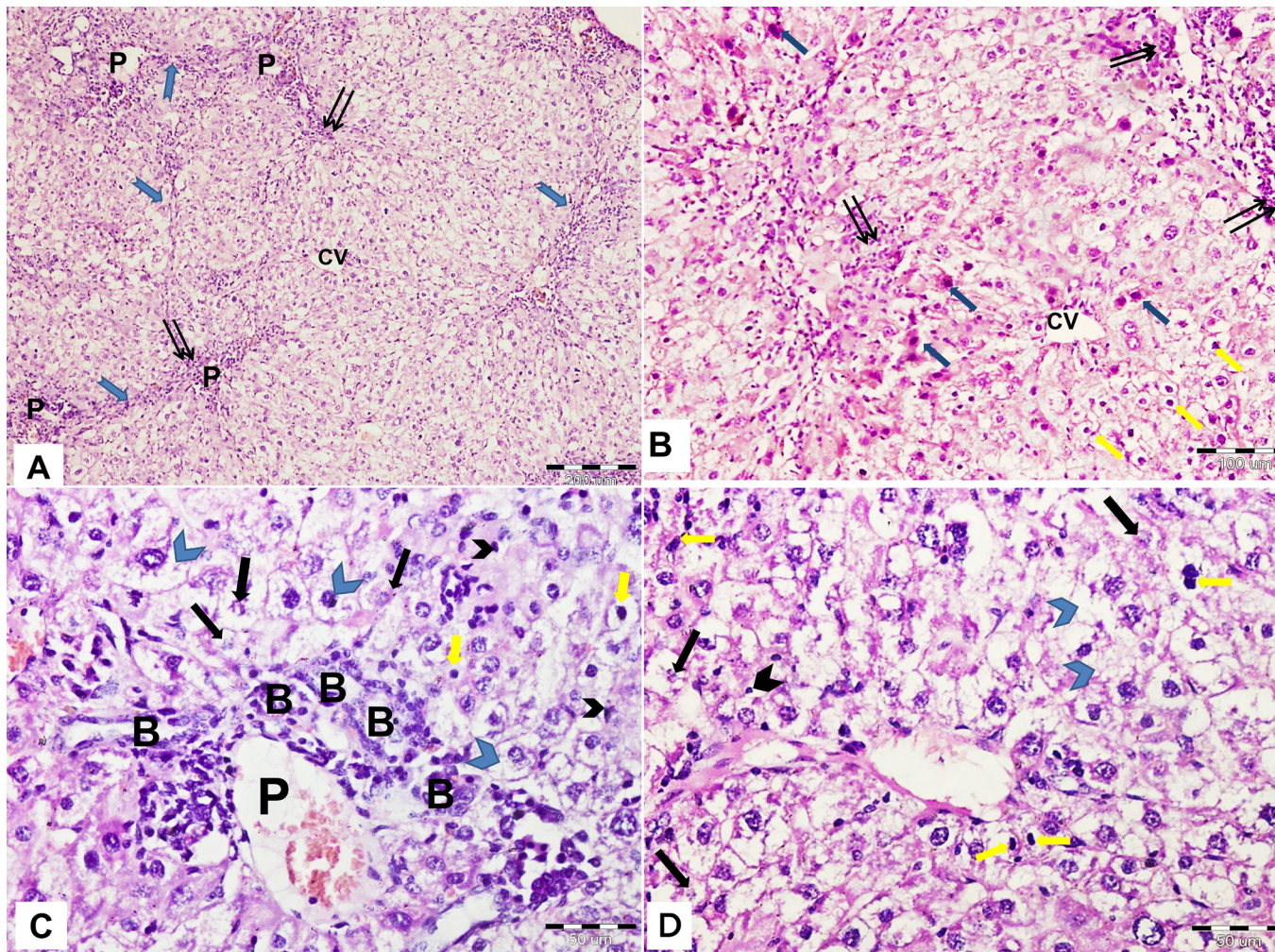


Fig. 5 (A-D): H&E-stained sections of group III given TAA showing: **A:** Connective tissue septa (notched blue arrow) bridging the portal tracts and associated with evident cellular infiltration are depicted (double arrow). CV; central vein, P; portal tract. **B:** Some hepatocytes show hyper-eosinophilic cytoplasm and deeply stained nuclei (blue arrow). Many hepatocytes appeared with deeply stained nuclei (yellow arrow). Double arrows; Cellular infiltration. **C:** The portal area (P) shows proliferation of the bile duct (B). Swollen hepatocytes with vacuolated cytoplasm (blue chevron arrow) and others show deeply stained nuclei (yellow arrow). Long black arrow; karyolytic nuclei, Black chevron arrow; Kupffer cells. **D:** Many hepatocytes are ballooned with vacuolated cytoplasm (blue chevron arrow). Some nuclei are karyolytic (long black arrow). Yellow arrow; deeply stained nuclei. Ax 100, Bx 200, C and D x 400.

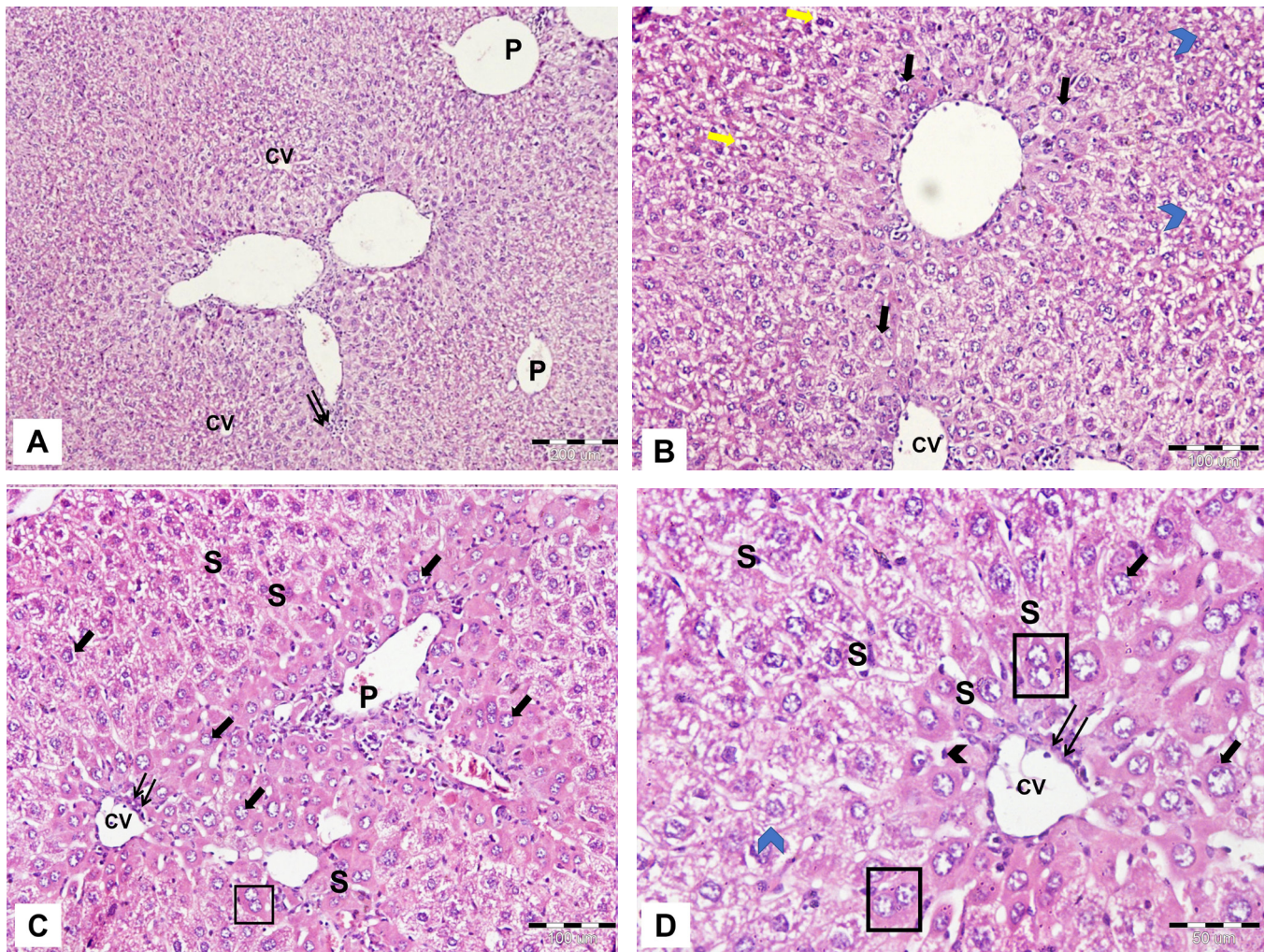


Fig. 6 (A-D): H&E-stained sections of the group IV (TAA+Alda-1 group) showing **A:** Regularly arranged hepatocytes radiating from the central vein (CV). Minimal cellular infiltration (double arrow) is also seen. P; portal tract. **B:** Hepatocytes are organized in cords. The cords are seen radiating from the central vein (CV). The majority of hepatocytes have eosinophilic cytoplasm and vesicular nuclei (black arrow). A few hepatocytes' cytoplasm is mildly vacuolated (blue chevron arrow). Yellow arrow; deeply stained nuclei. **C & D:** Most of the hepatocytes reveal vesicular nuclei and eosinophilic cytoplasm (black arrow). Some hepatocytes are binucleated (square). Minimal cellular infiltration (double arrow) is also seen. CV; central vein, S; hepatic sinusoid. P; portal tract in C. Blue chevron arrow; vacuolated cytoplasm in D, Black chevron arrow; Kupffer cells in D. Ax 100, C, B x200, Dx400.

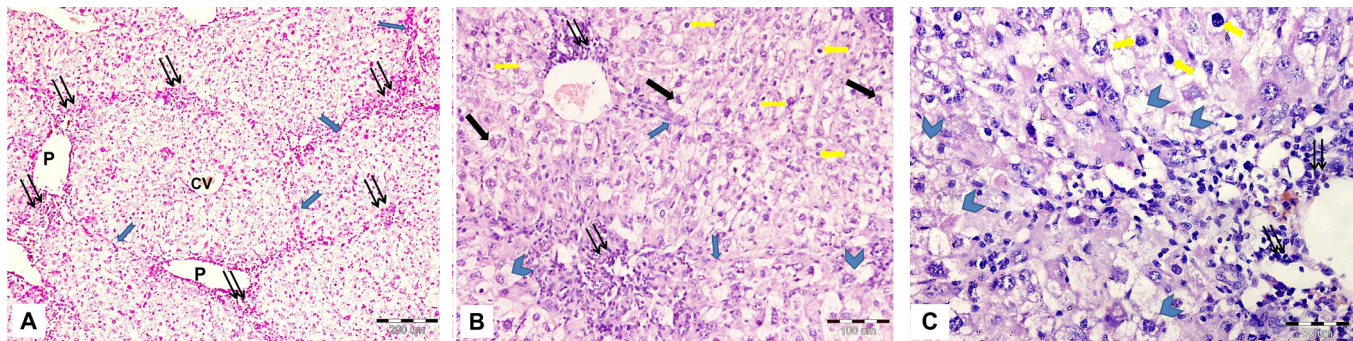


Fig. 7 (A-C): H&E-stained section of the recovery group showing **A:** Evident lobulation is seen. The connective tissue septa (notched blue arrow) are extending from one portal area to the other associated with cellular infiltration (double arrow). CV; central vein, P; portal tract. **B:** Hepatocytes show deeply stained nuclei (yellow arrow). Some hepatocytes have vacuolated cytoplasm (blue chevron arrow). Hepatocytes reveal karyolytic nuclei (black arrow). Double arrow; cellular infiltration. **C:** Hepatocytes are ballooned with vacuolated cytoplasm (blue chevron arrow). Many hepatocytes show deeply stained nuclei (yellow arrow). Double arrow; mononuclear cellular infiltration. Ax 100, Bx 200, Cx 400.

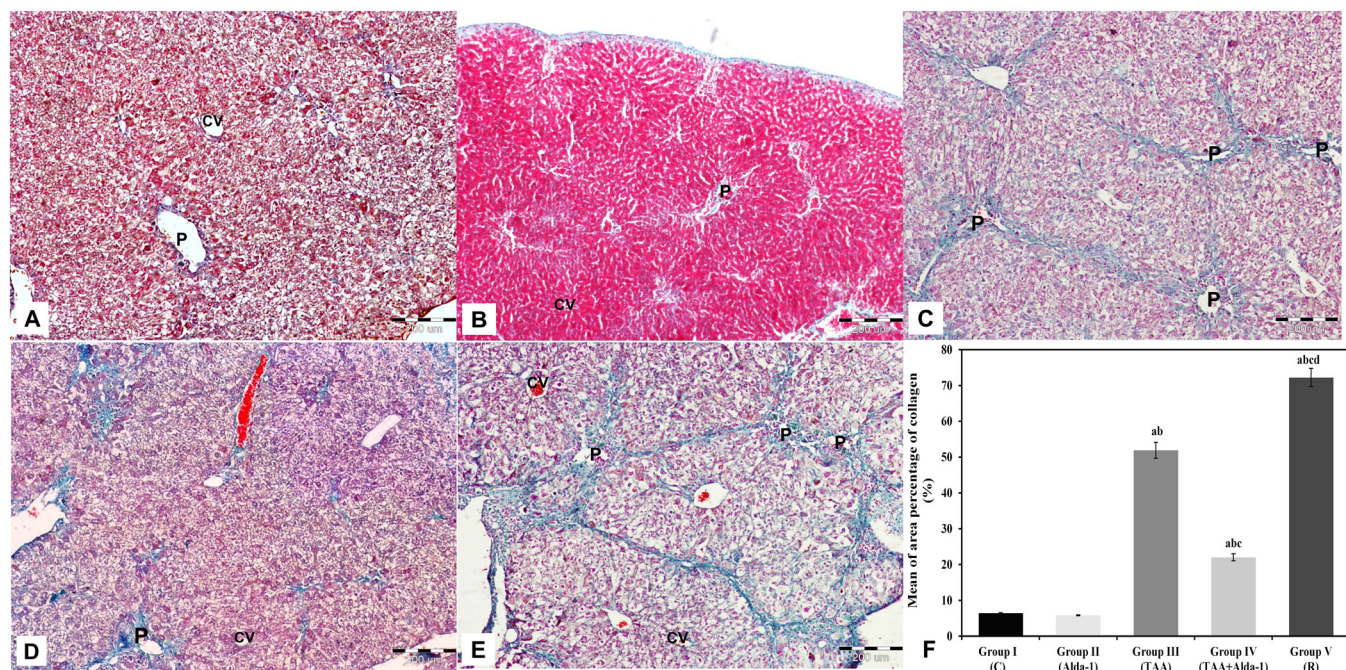


Fig. 8 (A-E): Masson's trichrome stained sections. **A:** Group I (control group): The stroma is seen to be formed of a scanty amount of collagen deposition that were prominent mainly around the components of the portal tract (P) and around the central vein (CV). **B:** group II (Alda-1 group): The liver is surrounded by a thin capsule. Minimal collagen deposition is seen surrounding the portal tract (P) and the central vein (CV). **C:** group III (TAA group): Connective tissue septa are seen strongly stained. In some areas, the septa are seen bridging from one portal tract (P) to the adjacent one. The distribution of collagen fibers is expanded extensively to be demonstrated between the hepatocytes. **D:** group IV (TAA+Alda-1 group): The liver sections show marked reduction of collagen deposition with only sporadic areas of collagen deposition around central vein and surrounding the components in the portal tract. **E:** group V (Recovery group): Examination demonstrates pronounced collagen deposition around the central veins and the portal tracts bridging from one portal tract to the other. A-Ex 100. **Fig. 8 F:** A bar chart demonstrating the morphometric statistical analysis comparison between the studied groups based on the mean area % of collagen deposition.

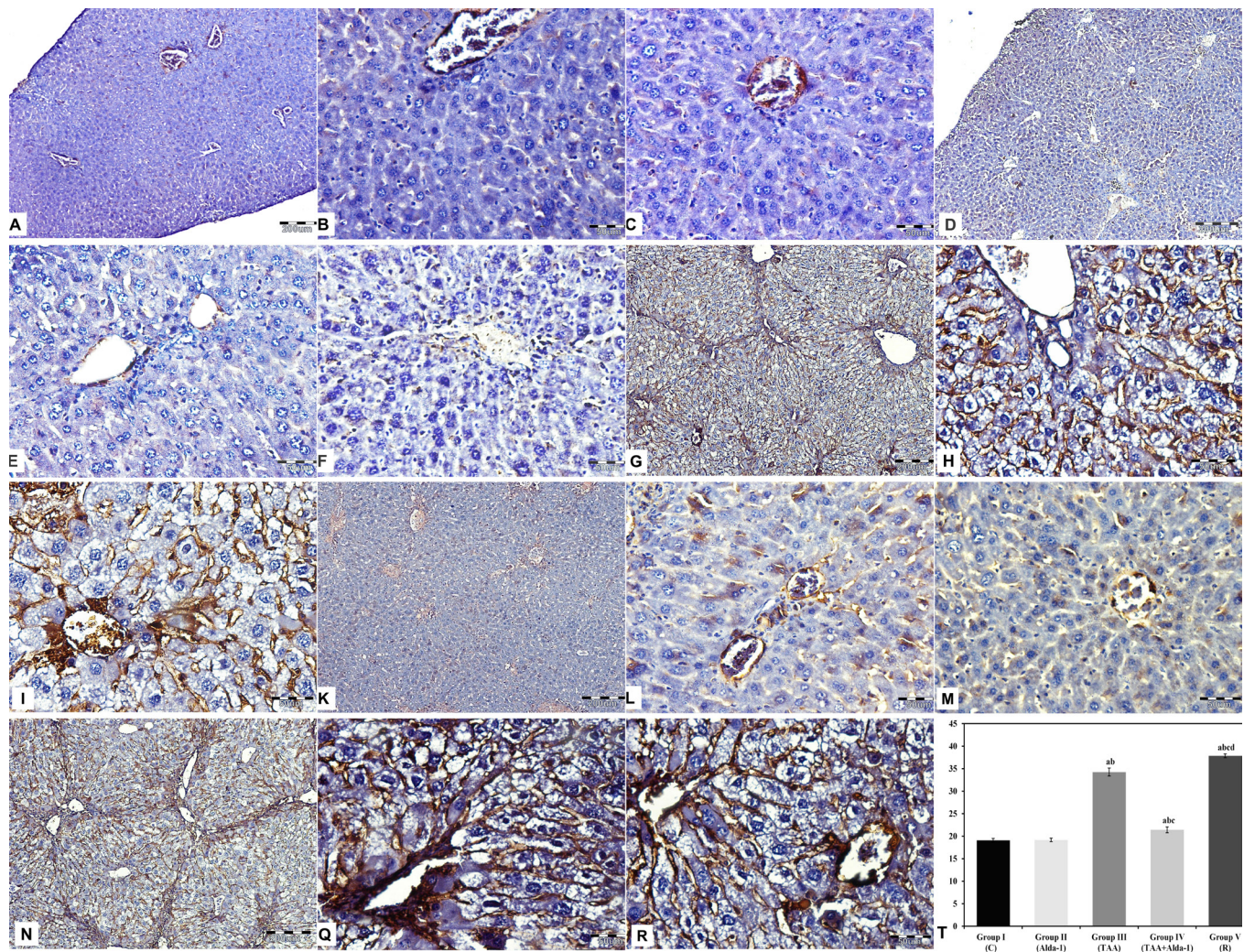


Fig. 9: (A-R) immunohistochemical stained sections of α -SMA expression. **A:** Group I (control group): Weak immunoreactivity for α -SMA is seen around the central veins and the vessels in the portal tracts. **B, C:** At higher magnification, the reaction is nearly negative between the hepatocytes. **D:** Group II (Alda-1 group): Weak immunoreaction around the portal tracts and the central veins. **E, F:** At higher magnification the reaction is negative in the perisinusoidal spaces between the hepatocytes. **G:** Group III (TAA group), showing increase reaction of α -SMA at the portal tracts and surrounding central veins and in the connective tissue septa as well. **H, I:** The reaction was also strong in the perisinusoidal spaces in between the hepatocytes. **K:** Group IV (TAA+Alda-1 group) showing marked reduction in the expression of α -SMA. **L, M:** At higher magnification the positive reaction is still seen in few perisinusoidal spaces in between the hepatocytes. **N:** Group V (recovery group) showing intense brown reaction of the α -SMA expression in the connective tissue septa from one portal tract to the adjacent portal tract giving a picture of lobulation. **Q, R:** Higher magnification reveals strong positive reaction in the perisinusoidal spaces between the hepatocytes, around the portal tract and around central vein. (α -SMA immunoreactivity. **A, D, G, K, N** x 100, **B, C, E, F, H, I, L, M, Q, R** x 400) **T:** A bar chart representing comparative morphometric statistical analysis between the studied groups according to the mean area % of α -smooth muscle actin expression.

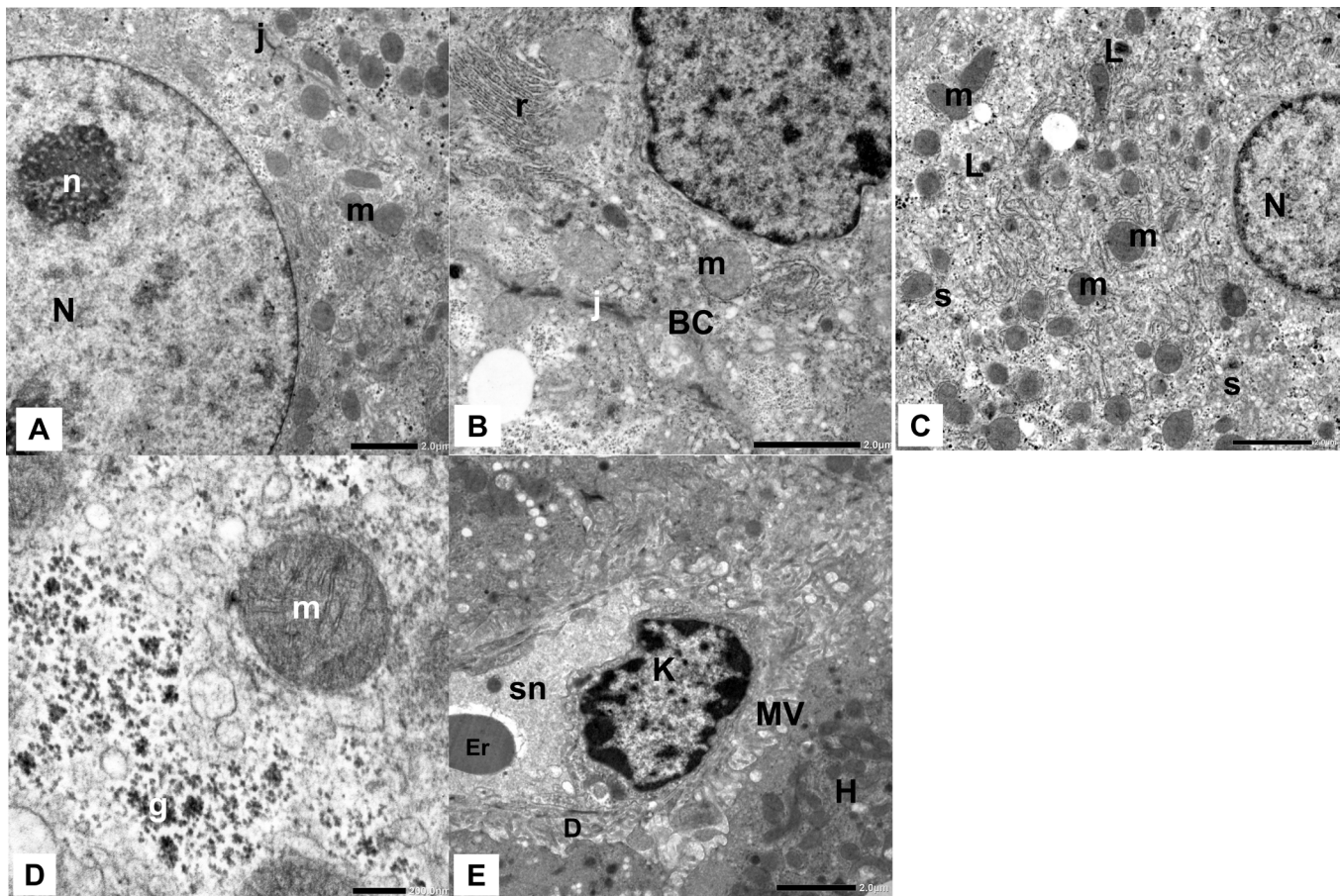


Fig. 10 (A-E): Electron micrographs of sections of the control group I **A:** Parts of two adjacent hepatocytes, one showing round euchromatic nucleus (N) and prominent nucleolus (n). The cytoplasm displays abundant mitochondria (m). J; tight junctions. **B:** The cytoplasm shows parallel profiles of rough endoplasmic reticulum (r). J; tight junctions, BC; bile canaliculus, m; mitochondria. **C:** The cytoplasm reveals mitochondria (m), tubular profiles of smooth endoplasmic reticulum (s) and few lysosomes (L). N; nucleus. **D:** The cytoplasm contains mitochondria (m) with prominent cristae. g; glycogen granules. **E:** Kupffer cell (K) is seen projecting in the lumen of a hepatic sinusoid (sn). H; part of a hepatocyte, MV; hepatic microvilli projecting in the space of Disse (D). Er; an erythrocyte. Ax 2500, B x 4000, Cx 3000, Dx20000, Ex3000.

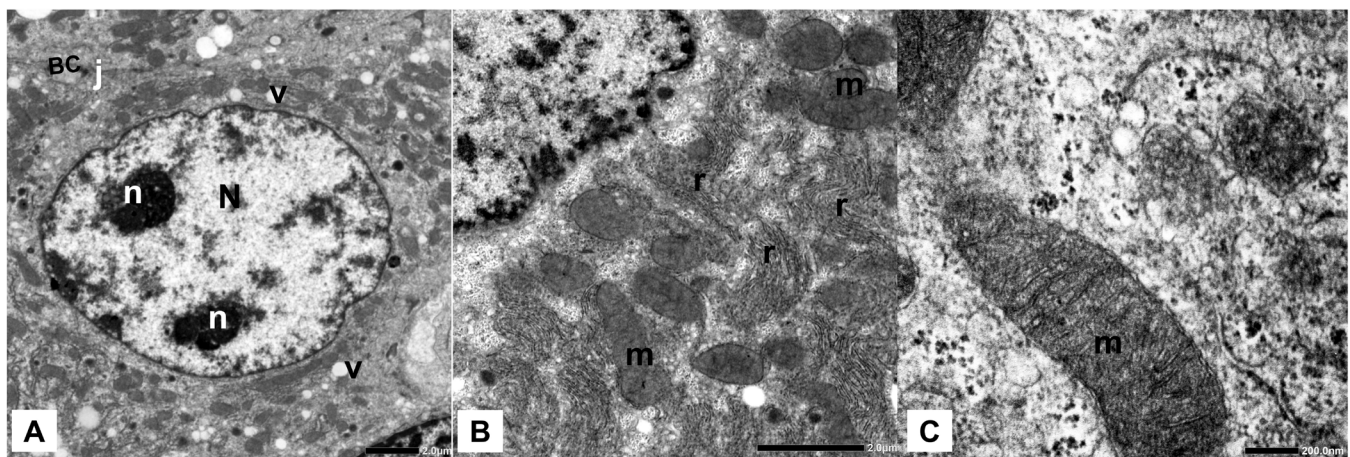


Fig. 11 (A-C): Electron micrographs of liver sections in group II receiving Alda-1 revealing: **A:** A hepatocyte having a central nucleus (N) with multiple nucleoli (n). V; vacuoles, BC; bile canaliculus, J; tight junctions. **B:** Numerous profiles of the rough endoplasmic reticulum (r) and mitochondria with prominent cristae (m). **C:** A high magnification showing a mitochondrion (m) with prominent cristae. Ax 2000, Bx 4000, Cx20000.

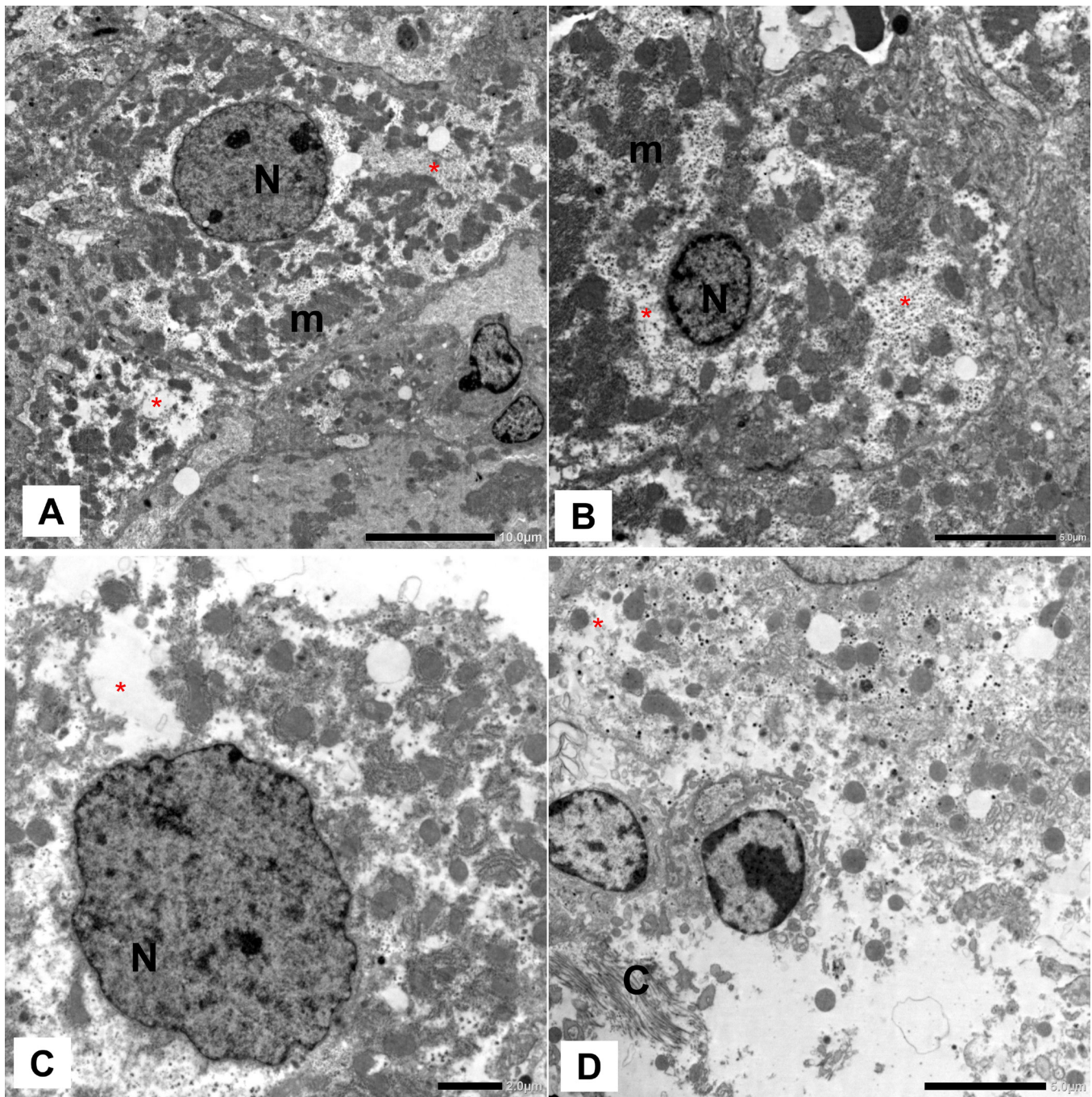


Fig. 12 (A-D): Electron micrographs of sections of the group III given TAA showing: **A, B:** Hepatocytes revealing marked cytoplasmic rarefaction (*). Mitochondria (m) with ill-defined limiting membrane are seen. The cytoplasmic organelles appear clumped together. N; nucleus. **C, D:** Rarefied cytoplasm (*) and disrupted cell membrane are seen. C; extracellular collagen fibrils in D. Ax800, B and Dx1500, Cx2000.

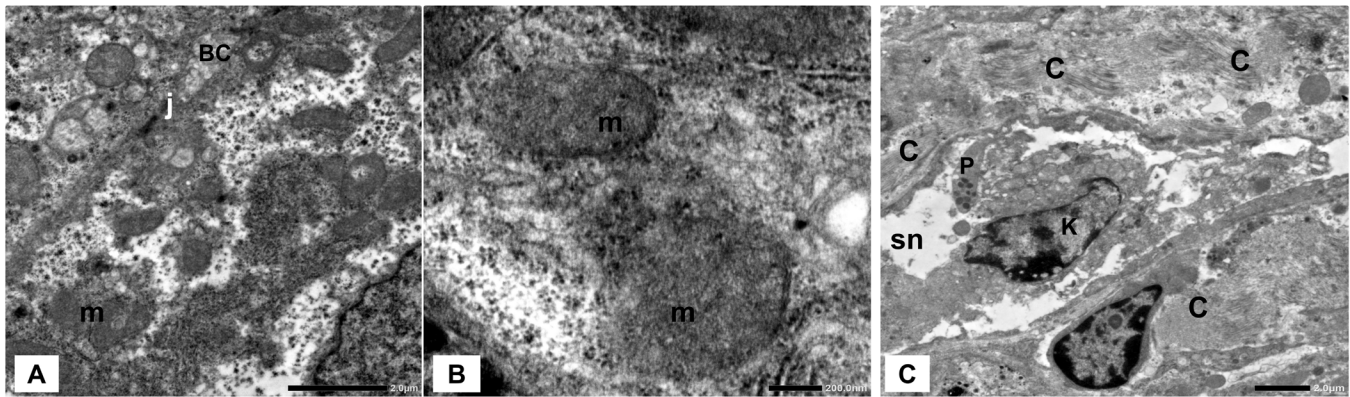


Fig. 13 (A-C): Electron micrographs of sections of the TAA group showing: **A:** Parts of two adjacent hepatocytes with a bile canaliculus (BC) between the two cells limited by tight junctions (j). Most of the cytoplasmic organelles are not well identified and clumped. m; Bizarre-shaped mitochondria. **B:** Mitochondria with disrupted membrane and ill-defined cristae (m). **C:** Perisinusoidal deposition of collagen fibrils (C). Sn; hepatic sinusoid, K; Kupffer cell, P; a blood platelet. Ax4000, Bx20000, Cx 2000.

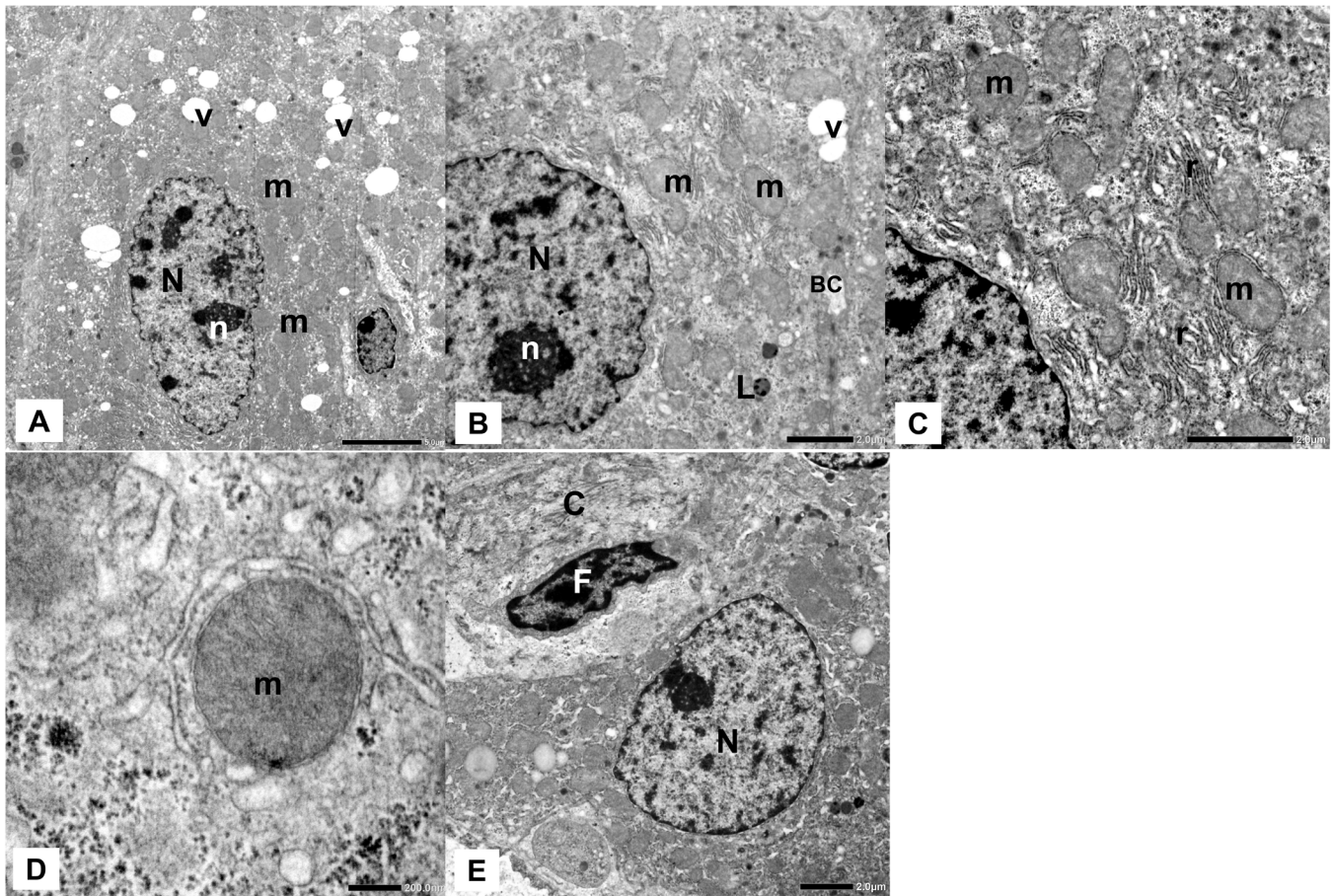


Fig. 14 (A-E): Electron micrographs of a section of the group IV received TAA+ Alda-1 showing **A, B:** reveal hepatocytes with euchromatic nucleus (N) having slightly irregular nuclear envelope and prominent nucleolus (n). The cytoplasm is heavily populated with mitochondria (m) with some vacuoles (V) are also depicted. Bile canaliculi (BC) can be seen between the two hepatocytes in B. L; Lysosome in B. **C:** Parallel cisternae of the rough endoplasmic reticulum (r). m; mitochondria. **D:** Mitochondrion (m) with intact outer membrane and prominent cristae. **E:** Part of a hepatocyte with a euchromatic nucleus (N). Few collagen fibrils (C) are seen adjacent to an elongated cell suggestive of a fibroblast (F). Ax 1200, Bx 2500, Cx 4000, Dx 20000, Ex 2000.

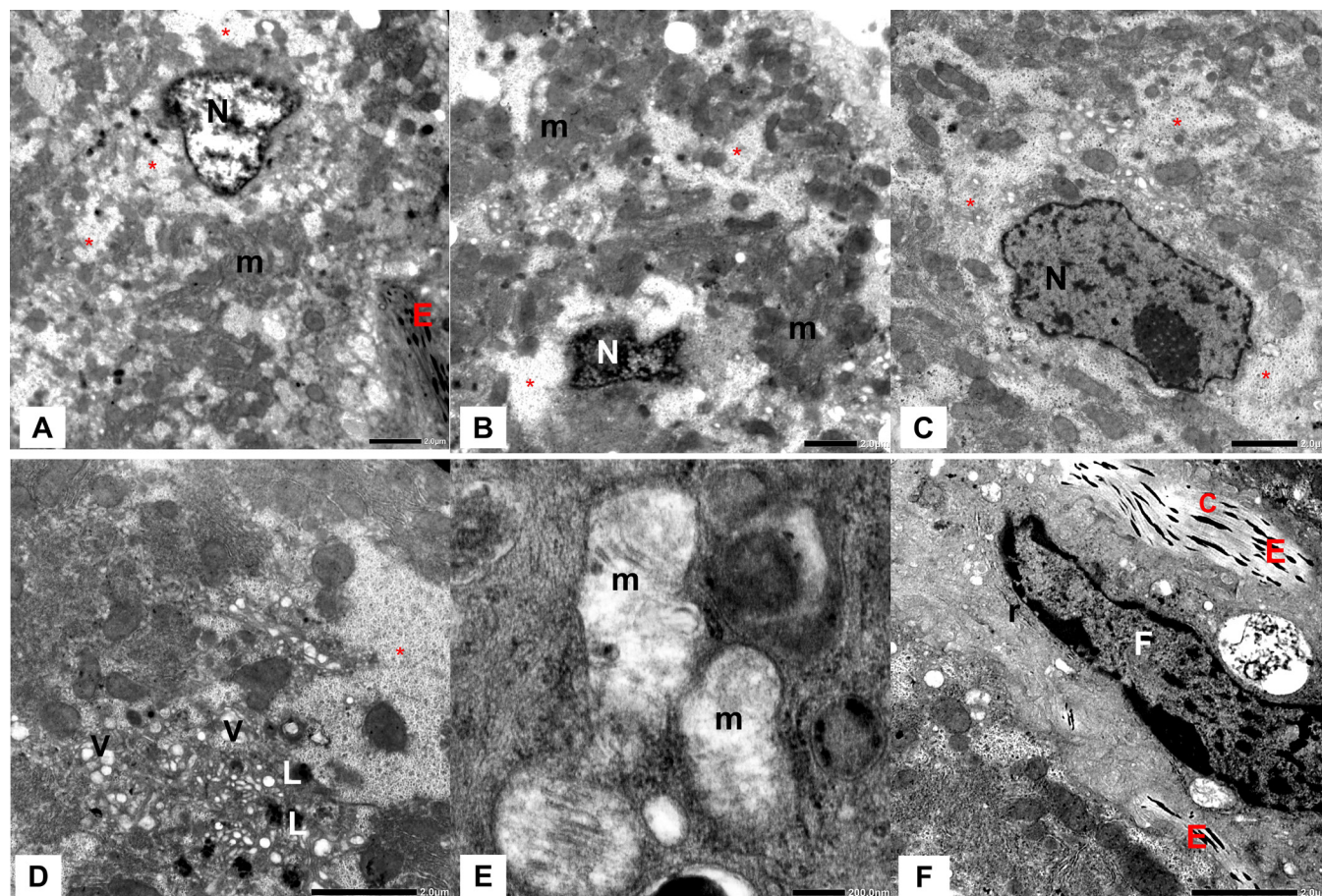


Fig. 15 (A-F): Electron micrographs of a section of group V showing: **A, B:** Hepatocytes having cytoplasmic rarefaction (*), irregular nucleus (N) and amalgamated mitochondria (m). Elastin (E) is seen extracellularly in A. **C, D:** Hepatocytes with cytoplasmic rarefaction (*). The cytoplasm reveals numerous lysosomes (L) and vacuoles (V) in D. **E:** Mitochondria (m) with loss of cristae are also seen. **F:** An elongated cell with elongated nucleus suggesting of an active secreting fibroblast (F) with extracellular collagen fibrils (C) intermingled with elastin (E). r: cisternae of rough endoplasmic reticulum. A and Bx 2000, Cx 2500, Dx 4000, Ex 20000, Fx4000.

DISCUSSION

The liver performs an important function in maintaining the overall homeostasis of the body, as well as the metabolism, storage, and redistribution of nutrients^[28]. Liver fibrosis is considered as one of the world's most common chronic diseases and it is linked to a high rate of morbidity and mortality^[29]. Among various hepatotoxic agents, thioacetamide (TAA) is recognized to be the most potent because of its outstanding solubility in water, and its cumulative effect^[30]. Moreover, experimentally initiated liver fibrosis by TAA administration results in biochemical and histological alterations as those of human liver fibrosis^[31,32].

In the current work, histological examination of group III (TAA) revealed disrupted liver architecture. Swollen, ballooned, and vacuolated cytoplasm and nuclear changes in the form of deep staining or karyolysis were seen, indicating degenerative alterations. Some hepatocytes showed hyper eosinophilic cytoplasm and deeply stained nuclei. Mitochondrial changes were another finding; they appeared pleomorphic, with loss of cristae and interrupted membrane. These findings were in line with researchers who investigated the production of liver fibrosis in experimental animals by TAA^[33,34].

TAA is metabolized by flavin-containing monooxygenase (FMO) system and cytochrome P450 enzymes (Cyt-p450) into reactive oxidative agents, thioacetamide sulfoxide (TAASO), and thioacetamide disulfoxide (TAASO₂)^[35]. Many researchers reported that TAA is responsible for nuclear changes, mitochondrial activity inhibition and changes in the cell permeability^[36,37]. Additionally, TAASO₂ is a very reactive compound that causes necrosis by targeting protein denaturation especially those involved in mitochondrial respiration and production of reactive oxygen species (ROS) such as hydrogen peroxide, super oxide anion O₂⁻, and the hydroxyl radical^[38,39]. ROS induce cell damage by induction of peroxidation of membrane lipids and DNA injury. This might explain the increased cytoplasmic eosinophilia after administration of TAA in group III^[40,41].

Peroxidation of membrane lipids leads also to the formation of reactive aldehydes such as 4-hydroxy-2-nonenal (4HNE) and malondialdehyde (MDA) that are considered the major peroxidation's primary end-product of polyunsaturated fatty acids, which further aggravates the injury^[42].

In the present study, induction of oxidative stress state has been proved by significant decrease in GSH and

increase in MDA levels in mice treated with TAA. These findings are in harmony with preceding studies^[43,44] which found that TAA's oxidative stress capability surpasses that of the cell's antioxidative and protective processes.

The significant increase in the serum levels of ALT and AST in the current study is regarded as a biomarker of hepatocytes' cell membrane damage. In accordance with the results of this study, researchers reported that these enzymes were statistically elevated in TAA-treated experimental mice^[45].

Presently the Ishak's scoring has been utilized to evaluate liver fibrosis. Where zero means absence of fibrosis, score one = expansion of some portal areas with connective tissue septa or without connective tissue septa, score two=expansion of most portal areas with connective tissue septa or without connective tissue septa, score three = expansion of majority of the portal areas with portal-to-portal bridging, score four= expansion of most portal areas with portal to portal and portal to central bridging, while score five = bridging with occasional nodules, and finally score 6 means cirrhosis^[46]. In the current study, fibrosis was detected, crossing from one portal area to the adjacent one (Ishak's score three by using the Masson's trichrome in group III. These results were confirmed by the histomorphometry analysis, and the area % of collagen that was significantly augmented in animals receiving TAA as compared to group I and group II (Ishak's scoring =zero).

One of the most critical processes in the progression of liver fibrosis is the activation of hepatic stellate cells (HSCs)^[47]. Upon liver injury, a complex signal promotes trans-differentiation of quiescent HSCs into myofibroblasts characterized by loss of retinoids and lipid droplets and expression of α -smooth muscle actin (α -SMA)^[48,49]. Activated HSCs promote synthesis of large amount of collagen especially collagen type I and other extracellular matrix (ECM) together with inhibition of matrix degradation^[50]. It was reported that hepatic fibrosis is commonly commenced by injury and damage of the hepatocytes, which causes Kupffer cells to activate and produce cytokines and growth factors^[51]. Among these growth factors is transforming growth factor β 1 (TGF- β 1), one of the extremely potent pro-fibrogenic mediators through Smad-dependent pathways. Preceding experiments have stated that the suppression of TGF- β 1/Smad signaling pathway reduces liver fibrosis^[52]. It also promotes fibroblast recruitment, proliferation, and differentiation into ECM- producing myofibroblast^[53]. It is well established that TGF- β 1 also increases the expression of α -SMA, a specific marker for identifying activated HSCs into myofibroblastic phenotype^[54,55]. Moreover, TGF- β 1 stimulates collagen gene transcription, which is abundantly expressed in activated HSCs^[56]. In the current work, TAA administration induced liver fibrosis (Ishak's score =three), which was manifested by significant increase in the area % of collagen deposition, TGF- β 1 level, and collagen- 1 gene expression. Immunohistochemically strong expression of α -SMA was detected and confirmed by the morphometric

analysis of the area percentage of α -SMA. Similar results have been reported by other researchers^[57].

Inflammation plays a significant impact in liver fibrosis. This was evident in the current study by the presence of cellular infiltration especially in the portal areas and increase in the levels of tissue TNF- α and of IL-6. Many studies proved that inflammation leads to secretion of cytokines and chemokines like TNF- α and IL-6 which promote liver fibrosis^[58-60]. Moreover, TAA has been proven to stimulate the expression of the nuclear factor-kappa B (NF- κ B), which in turn causes the production of inflammatory factors, namely TNF- α and IL-6 which are considered as primary biomarkers in acute inflammatory response^[61,62]. Another key aspect is oxidative stress, which aids in the activation of HSCs while also increasing collagen production^[63,64]. Several studies displayed that a vicious cycle was created. It is well documented that in liver fibrosis, oxidative stress and inflammatory mediators would trigger the activity of HSCs and contrariwise when the HSCs become activated this would boost the production of ROS, inflammatory response and hinder the antioxidant defenses of the cell^[65,66].

Evident proliferation of bile ducts was also noticed in the portal area of TAA treated animals. This was explained by some researchers that cholangiocytes might function as facultative stem cells and undergo trans-differentiation to rescue failed regeneration of hepatocytes^[67].

The best treatment of liver fibrosis is liver transplantation. However, transplantation constrained by high cost and a small donor base. Thus, alternative liver fibrosis management techniques are desperately needed^[68].

In the present study, administration of Alda-1 in group IV resulted in preservation of the histological structure of the liver together with significant decrease in AST and ALT levels in the sera of animals compared to group III (TAA group).

Alda-1 is an organic compound that improves the enzymatic activity of aldehyde dehydrogenase-2 (ALDH2), which in turn performs an important role in removing of endogenous aldehydes like 4HNE and MDA produced by lipid peroxidation provoked by oxidative stress^[42,69]. Liver contains many mitochondria, due to their great amounts of membranes and unsaturated phospholipids, mitochondria are well known as a major generator of ROS and a target for lipid peroxidation^[70]. Accordingly, activation of ALDH2 leads to increase clearance of aldehyde; therefore, Alda-1 is a promising therapy. Similarly, Alda-1 was found to boost ALDH2 activation by roughly threefold in mouse liver and isolated liver mitochondria^[71].

In the current work, a significant increase in GSH was linked to a significant reduction in the MDA levels in group IV (TAA+Alda-1 group). This was in accordance with many researchers who reported the defensive effect of Alda-1 in cardiac ischemia-reperfusion injury and dermatitis induced by radiation through insuring continuous detoxification of oxidative stress induced aldehydes^[72,73]. Moreover, TNF- α

and IL-6 levels were significantly decreased in group IV (TAA+Alda-1 group) compared to group III (TAA group). Another possible mechanism explaining the ameliorative effect of Alda-1 is its anti-inflammatory properties as it detoxifies reactive aldehydes which responsible for activation of NF- κ B pathway, the main activator for inflammatory response^[74,75]. Also, decreased area percentage of the collagen deposition and improvement in the level of fibrosis (Ishak's score one-two), α -SMA, TGF- β 1 levels and collagen-1 gene expression were reported in the present study. These findings were noticed by Ma *et al.*^[75] who studied the effect of Alda-1 in alleviating carbon tetrachloride (CCL4)-induced liver fibrosis through reduction of ROS production.

However, it is evident that in the group V (recovery group) histological changes persisted and the levels of liver transaminases continued progressing with sustained increase in TGF- β 1, collagen-1 gene expression and significant increase in the area % of α -SMA positive reaction and collagen deposition. The score of liver fibrosis was progressed from Ishak's score three in group III to score five in group V. In addition, the levels of TNF- α and IL-6 were significantly increased in comparison to the control group.

In early fibrosis, there is accumulation of collagen type I, III and fibronectin. As fibrosis progresses, the ECM accumulates with increasing the amount of type I collagen in addition to type IV fibrillar collagen and elastin which contributes to liver fibrosis progression^[76,77]. It was reported that elastin is highly expressed from the start of liver injury and that deposited elastin is very stable once constructed^[78]. In addition, it was demonstrated that elastin degrades slowly during recovery. Accumulation of collagen and elastin over a long period of time, leads to sequestrations of these fibers within the tissue beds making them inaccessible for proteolytic digestion^[79,80]. Moreover, previous studies declared that when the liver's elastin content accumulates, the ECM density and stiffness rise^[81,82]. This might explain the decreasing reversibility of fibrosis (Ishak's score five) with advancing time in group V (recovery group). This was associated with the elastin deposition that was demonstrated by the electron microscopic examination.

CONCLUSION

The results of the current research supported the potential hepatoprotective effect of Alda-1 in liver fibrosis after TAA administration. This protective effect was demonstrated histologically, immunohistochemically, and biochemically. The study depicted that this effect appeared to be mediated via its antioxidant, anti-inflammatory, and anti-fibrotic properties. This opens a way to focus more on Alda-1 as a promising drug in liver fibrosis. More studies on Alda-1 in the treatment of patients with liver fibrosis are recommended.

CONFLICT OF INTERESTS

There are no conflicts of interest.

REFERENCES

- Lambrecht J, van Grunsven LA and Tacke F. Current and emerging pharmacotherapeutic interventions for the treatment of liver fibrosis. *Expert. Opin. Pharmacother.* (2020)21(13):1637-1650.
- Kisseleva T and Brenner D. Molecular and cellular mechanisms of liver fibrosis and its regression. *Nat. Rev. Gastroenterol. Hepatol.* (2021)18(3):151-166.
- Yang H, Xuefeng Y, Shandong W and Jianhua X. COX-2 in liver fibrosis. *Clin. Chim. Acta.* (2020)506:196-203.
- An P, Wei LL, Zhao S, Sverdlov DY, Vaid KA, Miyamoto M, *et al.* Hepatocyte mitochondria-derived danger signals directly activate hepatic stellate cells and drive progression of liver fibrosis. *Nat. Commun.* (2020)11(1):2362.
- Tao Y, Wang N, Qiu T and Sun X. The Role of Autophagy and NLRP3 Inflammasome in Liver Fibrosis. *Biomed. Res. Int.* (2020)2020:7269150.
- Dai Z, Song G, Balakrishnan A, Yang T, Yuan Q, Möbus S, *et al.* Growth differentiation factor 11 attenuates liver fibrosis via expansion of liver progenitor cells. *Gut* (2020)69(6):1104-1115.
- Miao Y, Wu Y, Jin Y, Lei M, Nan J and Wu X. Benzoquinone derivatives with antioxidant activity inhibit activated hepatic stellate cells and attenuate liver fibrosis in TAA-induced mice. *Chem. Biol. Interact.* (2020)317:108945.
- Lee KC, Hsu WF, Hsieh YC, Chan CC, Yang YY, Huang YH, *et al.* Dabigatran Reduces Liver Fibrosis in Thioacetamide-Injured Rats. *Dig. Dis. Sci.* (2019)64(1):102-112.
- Elnfarawy AA, Nashy AE, Abozaid AM, Komber IF, Elweshahy RH and Abdelrahman RS. Vinpocetine attenuates thioacetamide-induced liver fibrosis in rats. *Hum. Exp. Toxicol.* (2021)40(2):355-368.
- Dwivedi DK, Jena G and Kumar V. Dimethyl fumarate protects thioacetamide-induced liver damage in rats: Studies on Nrf2, NLRP3, and NF- κ B. *J. Biochem. Mol. Toxicol.* (2020)34(6):e22476.
- Liu YC, Wang HL, Huang YZ, Weng YH, Chen RS, Tsai WC, *et al.* Alda-1, an activator of ALDH2, ameliorates Achilles tendinopathy in cellular and mouse models. *Biochem. Pharmacol.* (2020)175:113919.
- Sidramagowda Patil S, Hernández-Cuervo H, Fukumoto J, Krishnamurthy S, Lin M, Alleyn M, *et al.* Alda-1 Attenuates Hyperoxia-Induced Acute Lung Injury in Mice. *Front. Pharmacol.* (2021)11:597942.
- Zhang S, Chen C, Ying J, Wei C, Wang L, Yang Z, *et al.* Alda-1, an Aldehyde Dehydrogenase 2 Agonist, Improves Cutaneous Wound Healing by Activating Epidermal Keratinocytes via Akt/GSK-3 β /Catenin Pathway. *Aesthetic. Plast. Surg.* (2020)44(3):993-1005.

14. Liu Z, Ye S, Zhong X, Wang W, Lai CH, Yang W, *et al.* Pretreatment with the ALDH2 activator Alda 1 protects rat livers from ischemia/reperfusion injury by inducing autophagy. *Mol. Med. Rep.* (2020)22(3):2373-2385.
15. Salem AM, Mahdy KA, Hassan NS, El-Saeed GSM, Farrag AKH, Abdel Monem MA. Nigella sativa seed reduced galectin-3 level and liver fibrosis in thioacetamide-induced liver injury in rats. *J. Arab Society Med. Res.* (2017)12: 46 - 55.
16. Zhong W, Zhang W, Li Q, Xie G, Sun Q, Sun X, *et al.* Pharmacological activation of aldehyde dehydrogenase 2 by Alda-1 reverses alcohol-induced hepatic steatosis and cell death in mice. *J. Hepatol.* (2015)62(6):1375-1381.
17. Obi E, Egbuonu AC. Changes in the liver histomorphology, catalase and glutathione peroxidase activity in the serum and liver homogenate of normal and monosodium glutamate-intoxicated rats co-treated with artemether-lumefantrine. *Int J Mol Biol Open Access.* 2019;4(2):67-73.
18. Shareef SH, Ibrahim IA, Alzahrani AR, Al-Medhtiy MH, Abdulla MA. Hepatoprotective effects of methanolic extract of green tea against Thioacetamide-Induced liver injury in Sprague Dawley rats. *Saudi journal of biological sciences.* 2022 Jan 1;29(1):564-73..
19. Czechowska G, Celinski K, Korolczuk A, Wojcicka G, Dudka J, Bojarska A, *et al.* Protective effects of melatonin against thioacetamide-induced liver fibrosis in rats. *J. Physiol. Pharmacol.* (2015) 66(4):567-579.
20. Younis NS, Ghanim AM, Elmorsy MA and Metwaly HA. Taurine ameliorates thioacetamide induced liver fibrosis in rats via modulation of toll like receptor 4/ nuclear factor kappa B signaling pathway. *Sci. Rep.* (2021)11: 12296-12313.
21. Abdelaziz RR, Elkashef WF and Said E. Tranilast reduces serum IL-6 and IL-13 and protects against thioacetamide-induced acute liver injury and hepatic encephalopathy. *Environ. Toxicol. Pharmacol.* (2015)40: 259-267.
22. Yang HY, Kim KS, Lee YH, Park JH, Kim JH, Lee SY, *et al.* Dendropanax morbifera Ameliorates Thioacetamide-Induced Hepatic Fibrosis via TGF- β 1/Smads Pathways. *Int. J. Biol. Sci.* (2019)15(4):800-811.
23. Tong Z, Chen R, Alt DS, Kemper S, Perbal B and Brigstock DR. Susceptibility to liver fibrosis in mice expressing a connective tissue growth factor transgene in hepatocytes. *Hepatology* (2009)50(3):939-947.
24. Bancroft J and Layton C. The hematoxylin and eosin, connective and mesenchymal tissues with their stains. In: Suvarna S, Layton C and Bancroft J (eds). *Bancroft's Theory and Practice of Histological Techniques.* 7th ed. Churchill Livingstone. Philadelphia. (2013) pp: 173-212.
25. Graham R, Gray T, Bancroft J and Stevens A. *Electron microscopy 2: practical procedures.* In: Bancroft JD and Stevens A (eds). *Theory and Practice of Histological Techniques.* 4th ed. Churchill-Livingstone. New York. (1996) pp: 101-123.
26. Klein S, Hinüber C, Hittatiya K, Schierwagen R, Uschner FE, Strassburg CP, *et al.* Novel rat model of repetitive portal venous embolization mimicking human non-cirrhotic idiopathic portal hypertension. *PLoS One* (2016) 11: e0162144.
27. Kotz S, Balakrishnan N, Read C and Vidakovic B: *Encyclopedia of statistical sciences.* 2nd ed., Wiley-Interscience. Hoboken, N.J. (2006) pp 8371-8377.
28. Saneyasu T, Akhtar R, and Sakai T. Molecular cues guiding matrix stiffness in liver fibrosis. *BioMed. Res. Int.* (2016)2016: 2646212. Aydın MM and Akçalı KC. Liver fibrosis. *Turk. J. Gastroenterol.* (2018)29(1):14-21.
29. Al-Attar AM. Attenuating effect of Ginkgo biloba leaves extract on liver fibrosis induced by thioacetamide in mice. *J. Biomed. Biotechnol.* (2012)2012: 761450.
30. Abramovitch S, Dahan-Bachar L, Sharvit E, Weisman Y, Ben Tov A, Brazowski E, *et al.* Vitamin D inhibits proliferation and profibrotic marker expression in hepatic stellate cells and decreases thioacetamide-induced liver fibrosis in rats. *Gut* (2011)60(12): 1728–1737.
31. Liedtke C, Luedde T, Sauerbruch T, Scholten D, Streetz K, Tacke F, *et al.* Experimental liver fibrosis research: update on animal models, legal issues and translational aspects. *Fibrogenesis Tissue. Repair.* (2013)6(1):19.
32. Bilgiç Y, Harputluoglu M, Kutlu O, Demirel U, Gul M, Otlu B, *et al.* Effects of Lycium barbarum on bacterial translocation in thioacetamide-induced liver injury in rats. *Eur. J. Inflamm.* (2015)13:154-163.
33. Zargar S, Wani TA, Alamro AA and Ganaie MA. Amelioration of thioacetamide-induced liver toxicity in Wistar rats by rutin. *Int. J. Immunopathol. Pharmacol.* (2017)30(3):207-214.
34. Hajovsky H, Hu G, Koen Y, Sarma D, Cui W, Moore DS, *et al.* Metabolism and toxicity of thioacetamide and thioacetamide S-oxide in rat hepatocytes. *Chem. Res. Toxicol.* (2012)25: 1955–1963.
35. Koen YM, Sarma D, Hajovsky H, Galeva NA, Williams TD, Staudinger JL, *et al.* Protein targets of thioacetamide metabolites in rat hepatocytes. *Chem. Res. Toxicol.* (2013)26(4):564-574.
36. Prabha SP, Ansil PN, Nitha A, Wills PJ and Latha MS. Preventive and curative effect of methanolic extract of Gardenia gummifera Linn. f. on thioacetamide induced oxidative stress in rats. *Asian Pac. J. Trop. Dis.* (2012)2(2):90-98.

37. Schieber M, Chandel NS. ROS function in redox signaling and oxidative stress. *Current biology*. 2014 May 19;24(10):R453-62..
38. Serviddio G, Bellanti F and Vendemiale G. Free radical biology for medicine: learning from nonalcoholic fatty liver disease. *Free Radic. Biol. Med.* (2013)65: 952-968.
39. Alshawsh MA, Abdulla MA, Ismail S and Amin ZA. Hepatoprotective Effects of Orthosiphon stamineus Extract on Thioacetamide-Induced Liver Cirrhosis in Rats. *Evid. Based Complement. Alternat. Med.* (2011)2011:103039.
40. Arroyave-Ospina JC, Wu Z, Geng Y and Moshage H. Role of oxidative stress in the pathogenesis of non-alcoholic fatty liver disease: implications for prevention and therapy. *Antioxidants (Basel)* (2021)10(2):174.
41. Bekyarova G, Tzaneva M, Bratoeva K, Ivanova I, Kotzev A, Hristova M, *et al.* 4-Hydroxynonenal (HNE) and hepatic injury related to chronic oxidative stress. *Biotechnol. Equip.* (2019)33(1): 1544-1552.
42. Wang JH, Hwang SJ and Son CG. Comparative analysis of the antioxidative and hepatoprotective activities of dimethyl diphenyl bicarboxylate in four animal models of hepatic injury. *Antioxidants* (2021)10: 1508- 1521.
43. Türkmen NB, Yüce H, Taşlıdere A, Şahin Y and Çiftçi O. The Ameliorate Effects of Nerolidol on Thioacetamide-induced Oxidative Damage in Heart and Kidney Tissue. *Turk. J. Pharm. Sci.* (2022)19(1):1-8.
44. Lin YY, Hu CT, Sun DS, Lien TS and Chang HH. Thioacetamide-induced liver damage and thrombocytopenia is associated with induction of antiplatelet autoantibody in mice. *Sci. Rep.* (2019) 9:17497.
45. Wang H, Zhang H, Wang Y, Yang L, Wang D. Embelin can protect mice from thioacetamide-induced acute liver injury. *Biomed Pharmacother.* (2019); 118: 109360.
46. Germani G, Burroughs AK, Dhillon AP. The relationship between liver disease stage and liver fibrosis: a tangled web. *Histopathology.* (2010);57:773-84.
47. Wang H, Zheng S, Jiang H, Wang X, Zhou F and Weng Z. Single-cell transcriptomic analysis reveals a novel cell state and switching genes during hepatic stellate cell activation *in vitro*. *J. Transl. Med.* (2022) 20:53-66.
48. Higashi T, Friedman SL and Hoshida Y. Hepatic stellate cells as key target in liver fibrosis. *Adv. Drug Deliv. Rev.* (2017)121: 27-42.
49. Roderfeld M. Matrix metalloproteinase functions in hepatic injury and fibrosis. *Matrix. Biol.* (2018)68-69:452-462.
50. Lee UE, Friedman SL. Mechanisms of hepatic fibrogenesis. *Best practice & research Clinical gastroenterology.* 2011 Apr 1;25(2):195-206.
51. Jing Wu , Lin PanI, Xueqin Jin, Weihua Li, Hongbing Li , Jianmao Chen, *et al.* The role of oxymatrine in regulating TGF-β1 in rats with hepatic fibrosis. *Acta Cir Bras.* 2018;33(3):207-215.
52. Fabregat I, Moreno-Càceres J, Sánchez A, Dooley S, Dewidar B, Giannelli G, *et al.* IT-LIVER Consortium. TGF-β signalling and liver disease. *FEBS J.* (2016)283(12):2219-2232.
53. Yang Y, Sun M, Li W, Liu C, Jiang Z, Gu P, *et al.* Rebalancing TGF-β/Smad7 signaling via Compound kushen injection in hepatic stellate cells protects against liver fibrosis and hepatocarcinogenesis. *Clin. Transl. Med.* (2021)11(7):e410.
54. Fan W, Liu T, Chen W, Hammad S, Longerich T, Hausser I, *et al.* ECM1 Prevents Activation of Transforming Growth Factor β, Hepatic Stellate Cells, and Fibrogenesis in Mice. *Gastroenterology* (2019)157(5):1352-67.e13.
55. Meng XM, Nikolic-Paterson DJ and Lan HY. TGF-β: the master regulator of fibrosis. *Nat. Rev. Nephrol.* (2016)12(6):325-338.
56. Arauz J, Moreno MG, Cortés-Reynosa P, Salazar EP and Muriel P. Coffee attenuates fibrosis by decreasing the expression of TGF-β and CTGF in a murine model of liver damage. *J. Appl. Toxicol.* (2013 33(9):970-979.
57. Rockey DC, Du Q, Weymouth ND and Shi Z. Smooth muscle α-actin deficiency leads to decreased liver fibrosis via impaired cytoskeletal signaling in hepatic stellate cells. *Am. J. Pathol.* (2019)189(11): 2209-2220.
58. Kakino S, Ohki T, Nakayama H, Yuan X, Otabe S, Hashinaga T, *et al.* Pivotal role of TNF-alpha in the development and progression of nonalcoholic fatty liver disease in a murine model. *Horm. Metab. Res.* (2018)50: 80-87.
59. Fielding CA, Jones GW, McLoughlin RM, McLeod L, Hammond VJ, Uceda J, *et al.* Interleukin-6 signaling drives fibrosis in unresolved inflammation. *Immunity* (2014)40: 40-50.
60. Shen H, Sheng L, Chen Z, Jiang L, Su H, Yin L, *et al.* Mouse hepatocyte overexpression of NF-κB-inducing kinase (NIK) triggers fatal macrophage-dependent liver injury and fibrosis. *Hepatology* (2014)60(6):2065-2076.

61. Amanzada A, Moriconi F, Mansuroglu T, Cameron S, Ramadori G and Malik IA. Induction of chemokines and cytokines before neutrophils and macrophage recruitment in different regions of rat liver after TAA administration. *Lab. Invest.* (2014)94(2):235-247.
62. Ramos-Tovar E, Muriel P. Molecular mechanisms that link oxidative stress, inflammation, and fibrosis in the liver. *Antioxidants*. 2020 Dec;9(12):1279.
63. Lan T, Kisseleva T and Brenner DA. Deficiency of NOX1 or NOX4 prevents liver inflammation and fibrosis in mice through inhibition of hepatic stellate cell activation. *Plos One* (2015)10:e0129743.
64. Lavieri R, Piccioli P, Carta S, Delfino L, Castellani P and Rubartelli A. TLR costimulation causes oxidative stress with unbalance of proinflammatory and anti-inflammatory cytokine production. *J. Immunol.* (2014)192(11):5373-5381.
65. Li S, Tan HY, Wang N, Zhang ZJ, Lao L, Wong CW, *et al.* The Role of oxidative stress and antioxidants in liver diseases. *Int. J. Mol. Sci.* (2015)16: 26087–26124.
66. Michalopoulos GK and Khan Z. Liver stem cells: experimental findings and implications for human liver disease. *Gastroenterology* (2015)149(4):876-882.
67. Crespo Yanguas S, Cogliati B, Willebrords J, Maes M, Colle I, Van den Bossche B, *et al.* Experimental models of liver fibrosis. *Arch. Toxicol.* (2016)90(5):1025-1048.
68. Wimborne HJ, Takemoto K, Woster PM, Rockey DC, Lemasters JJ and Zhong Z. Aldehyde dehydrogenase-2 activation by Alda-1 decreases necrosis and fibrosis after bile duct ligation in mice. *Free Radic. Biol. Med.* (2019)145:136-145.
69. Bulua AC, Simon A, Maddipati R, Pelletier M, Park H, Kim KY, *et al.* Mitochondrial reactive oxygen species promote production of proinflammatory cytokines and are elevated in TNFR1-associated periodic syndrome (TRAPS). *J. Exp. Med.* (2011)208(3):519-533.
70. Wang W, Wang C, Xu H, Gao Y. Aldehyde dehydrogenase, liver disease and cancer. *International Journal of Biological Sciences*. 2020;16(6):921.
71. Panisello-Roselló A, Lopez A, Folch-Puy E, Carbonell T, Rolo A, Palmeira C, *et al.* Role of aldehyde dehydrogenase 2 in ischemia reperfusion injury: An update. *World J. Gastroenterol.* (2018)24(27):2984.
72. Zhu Q, He G, Wang J, Wang Y and Chen W. Pretreatment with the ALDH2 agonist Alda-1 reduces intestinal injury induced by ischaemia and reperfusion in mice. *Clin. Sci.* (2017)131(11):1123-1136.
73. Fu SH, Zhang HF, Yang ZB, Li TB, Liu B, Lou Z, *et al.* Alda-1 reduces cerebral ischemia/reperfusion injury in rat through clearance of reactive aldehydes. *Naunyn-Schmiedeberg's Arch. Pharmacol.* (2014)387(1):87-94.
74. Shoeb M, Ansari NH, Srivastava SK and Ramana KV. 4-Hydroxynonenal in the pathogenesis and progression of human diseases. *Curr. Med. Chem.* (2014)21(2):230-237.
75. Ma X, Luo Q, Zhu H, Liu X, Dong Z, Zhang K, *et al.* Aldehyde dehydrogenase 2 activation ameliorates CCl4-induced chronic liver fibrosis in mice by up-regulating Nrf2/HO-1 antioxidant pathway. *J. Cell. Mol. Med.* (2018)22(8):3965-3978.
76. Pellicoro A, Aucott RL, Ramachandran P, Robson AJ, Fallowfield JA, Snowdon VK, *et al.* Elastin accumulation is regulated at the level of degradation by macrophage metalloelastase (MMP-12) during experimental liver fibrosis. *Hepatology* (2012)55(6):1965-1975.
77. Pellicoro A, Ramachandran P and Iredale JP. Reversibility of liver fibrosis. *Fibrogenesis Tissue Repair* (2012)5(Suppl 1):S26.
78. Kanta J. Elastin in the Liver. *Front. Physiol.* (2016)7:491.
79. Chen W, Yan X, Xu A, Sun Y, Wang B, Huang T, *et al.* Dynamics of elastin in liver fibrosis: Accumulates late during progression and degrades slowly in regression. *J. Cell. Physiol.* (2019)234:22613–22622.
80. Zhao W, Yang A, Chen W, Wang P, Liu T, Cong M, *et al.* Inhibition of lysyl oxidase-like 1 (LOXL1) expression arrests liver fibrosis progression in cirrhosis by reducing elastin crosslinking. *Biochim. Biophys. Acta Mol. Basis. Dis.* (2018)1864(4 Pt A):1129-1137.
81. Kendall TJ, Dolman GE, Duff CM, Paish EC, Zaitoun A, Irving W, *et al.* Hepatic elastin content is predictive of adverse outcome in advanced fibrotic liver disease. *Histopathology* (2018)73(1):90-100.
82. Baiocchini A, Montaldo C, Conigliaro A, Grimaldi A, Correani V, Mura F, *et al.* Extracellular matrix molecular remodeling in human liver fibrosis evolution. *PLoS One* (2016)11(3):e0151736.

المخلص العربي

القدرة التحسينية المحتملة لـ الدا-١ على تليف الكبد المستحدث لذكور الفئران البالغة. دراسة هيستولوجية وهيستوكيميائية مناعية وكيميائية

أماني عبد المنعم سليمان وسيلفيا كميل صديق ساويرس

قسم علم الأنسجة وبيولوجيا، الخلية، كلية الطب، جامعة الإسكندرية

المقدمة: يعتبر مرض تليف الكبد من الامراض التي لا يوجد لها علاج ثابت، بسبب طريقة تطور المرض المعقدة. يعتبر الدا-١ دواء واعداء في تحسين ذلك التليف.

الهدف من البحث: تقييم القدرة التحسينية المحتملة لـ الدا-١ على تليف الكبد المستحدث بالثيواسيتاميد في ذكور الفئران. **مواد وطرق البحث:** تم تقسيم خمس وعشرون من ذكور الفئران البالغة (٢٥-٢٧ جرام و ٢-٣ شهور) إلى خمس مجموعات متساوية. المجموعة الأولى (المجموعة الضابطة) و المجموعة الثانية (مجموعة الدا-١) (تلقت الدا-١) ٥ مجم / كجم، حقنا بالغشاء البروتوني مرتين أسبوعياً لمدة ٤ أسابيع. المجموعة الثالثة (مجموعة الثيواسيتاميد) تلقت الثيواسيتاميد (٢٠٠ مجم/كجم، حقنا بالغشاء البروتوني) مرتين أسبوعياً لمدة ٧ أسابيع. اما المجموعة الرابعة (مجموعة لثيواسيتاميد+ الدا-١): فقد تلقت جرعة الثيواسيتاميد كالمجموعة الثالثة. وبعد التوقف عن إعطاء الثيواسيتاميد، تم إعطاء الدا-١ بجرعة كالمجموعة الثانية واستمر لمدة ٤ أسابيع. اما المجموعة الخامسة (مجموعة التعافي) تلقت الثيواسيتاميد كالمجموعة الثالثة وتركت دون أي علاج لمدة ٤ أسابيع إضافية. تم الكشف عن التغيرات النسيجية عن طريق الميكروسكوب الضوئي (باستخدام صبغة الهيماتوكسلين والايوسين وصبغة ماسون ثلاثية الأوان) والميكروسكوب الإلكتروني والتحليل الكيميائي المناعي والمورفومتري. تم اخذ عينات من الدم لتقييم وظائف الكبد.

النتائج: تسبب الثيواسيتاميد في تغير نسيجي وكيميائي ملحوظ لبنية خلايا الكبد ووظيفتها مع زيادة كبيرة في ترسب الكولاجين. بالإضافة إلى ذلك، تسبب الثيواسيتاميد في ارتفاع كبير في إنزيمات الكبد.

أدى إعطاء الدا-١ إلى انخفاض ملحوظ من لإنزيمات الكبد المرتفعة مع تحسن ملحوظ في بنية خلايا الكبد وزيادة في الجلوتاثيون وانخفاض في ميلانودايهيدريد في أنسجة الكبد كما قلل الدا-١ من عامل النمو المحول المرتفع، والتعبير الحيني للكولاجين ١ في أنسجة الكبد ونسبة ترسب الكولاجين. بالإضافة إلى ذلك، تم تقليل بروتين الفا اكتين الخاص بالخلايا العضلية الملساء بشكل ملحوظ. تم الكشف عن التأثيرات المضادة للالتهابات أيضاً عن طريق انخفاض عامل انترليوكن ٦ وعامل نخر الورم ألفا في أنسجة الكبد.

الخلاصة: قلل الدا-١ من تليف الكبد الناجم عن الثيواسيتاميد في الفئران. قد يكون هذا بسبب آثاره المضادة للأكسدة والمضادة للتليف والالتهابات.